

University of Windsor

## Scholarship at UWindor

---

Electronic Theses and Dissertations

Theses, Dissertations, and Major Papers

---

1999

### Vibrational characterization of a series of aromatic quinones

William J. Price  
*University of Windsor*

Follow this and additional works at: <https://scholar.uwindsor.ca/etd>

---

#### Recommended Citation

Price, William J., "Vibrational characterization of a series of aromatic quinones" (1999). *Electronic Theses and Dissertations*. 4523.

<https://scholar.uwindsor.ca/etd/4523>

This online database contains the full-text of PhD dissertations and Masters' theses of University of Windsor students from 1954 forward. These documents are made available for personal study and research purposes only, in accordance with the Canadian Copyright Act and the Creative Commons license—CC BY-NC-ND (Attribution, Non-Commercial, No Derivative Works). Under this license, works must always be attributed to the copyright holder (original author), cannot be used for any commercial purposes, and may not be altered. Any other use would require the permission of the copyright holder. Students may inquire about withdrawing their dissertation and/or thesis from this database. For additional inquiries, please contact the repository administrator via email ([scholarship@uwindsor.ca](mailto:scholarship@uwindsor.ca)) or by telephone at 519-253-3000ext. 3208.

# VIBRATIONAL CHARACTERIZATION OF A SERIES OF AROMATIC QUINONES

by

William J. Price

A Thesis

Submitted to the Faculty of Graduate Studies and Research  
through the Department of Chemistry and Biochemistry  
in Partial Fulfillment of the Requirements for  
the Degree of Master of Science at the  
University of Windsor

Windsor, Ontario, Canada

1998

© 1998 William J. Price



Library and  
Archives Canada

Bibliothèque et  
Archives Canada

Published Heritage  
Branch

Direction du  
Patrimoine de l'édition

395 Wellington Street  
Ottawa ON K1A 0N4  
Canada

395, rue Wellington  
Ottawa ON K1A 0N4  
Canada

*Your file* *Votre référence*

*ISBN: 0-494-00130-5*

*Our file* *Notre référence*

*ISBN: 0-494-00130-5*

#### NOTICE:

The author has granted a non-exclusive license allowing Library and Archives Canada to reproduce, publish, archive, preserve, conserve, communicate to the public by telecommunication or on the Internet, loan, distribute and sell theses worldwide, for commercial or non-commercial purposes, in microform, paper, electronic and/or any other formats.

The author retains copyright ownership and moral rights in this thesis. Neither the thesis nor substantial extracts from it may be printed or otherwise reproduced without the author's permission.

#### AVIS:

L'auteur a accordé une licence non exclusive permettant à la Bibliothèque et Archives Canada de reproduire, publier, archiver, sauvegarder, conserver, transmettre au public par télécommunication ou par l'Internet, prêter, distribuer et vendre des thèses partout dans le monde, à des fins commerciales ou autres, sur support microforme, papier, électronique et/ou autres formats.

L'auteur conserve la propriété du droit d'auteur et des droits moraux qui protègent cette thèse. Ni la thèse ni des extraits substantiels de celle-ci ne doivent être imprimés ou autrement reproduits sans son autorisation.

---

In compliance with the Canadian Privacy Act some supporting forms may have been removed from this thesis.

Conformément à la loi canadienne sur la protection de la vie privée, quelques formulaires secondaires ont été enlevés de cette thèse.

While these forms may be included in the document page count, their removal does not represent any loss of content from the thesis.

Bien que ces formulaires aient inclus dans la pagination, il n'y aura aucun contenu manquant.

  
**Canada**

This dissertation was approved by:

---

R. Aroca, Dept. of Chemistry and Biochemistry

---

P. Dutton, Dept. of Chemistry and Biochemistry

---

M. Schlessinger, Dept. of Physics

---

## Abstract

The vibrational characterization of a series of molecules: 1,4-anthracenedione, 5,14-pentacenedione, 6,15-hexacenedione, 8,13-benzo[a]naphthacenedione, 7-methyl-8,13-benzo[a]naphthacenedione has been carried out. The synthesis of these materials was carried out in the research laboratory of Dr. P.Dibble of the Department of Chemistry, University of Lethbridge, Lethbridge, Alberta, who provided to us a purified sample of each compound. The inelastic scattering was measured at 1064nm (FT-Raman) and the infrared absorption spectra were measured in the mid-infrared (300-3600  $\text{cm}^{-1}$ ). The vibrational assignments of normal modes was assisted by semi-empirical quantum calculations with the AM1 and PM3 Hamiltonian. A high level ab initio computation for 5,14-pentacenedione is also reported. The thesis also contributes to the modern field of surface-enhanced vibrational spectroscopy (SEVS). Surface-enhanced Raman scattering (SERS) of vacuum evaporated quinone films and of single LB monolayers were obtained for some members of the series. For the first time, it has been observed that tin island films used in surface-enhanced infrared (SEIR) experiments give rise to an electromagnetic enhancement of the infrared absorption spectrum. The surface-enhancement of the infrared absorption by tin island films is shown for evaporated nanometric films of 5,14-pentacenedione (Q2). The SEIR enhancement was tuned by fabricating tin island films of varying mass thickness to achieve maximum enhancement. The film morphology was determined by transmission electron microscopy. Comparisons were made between the SEIR spectra on rough tin and on rough silver surfaces and the corresponding reflection-absorption infrared spectra (RAIRS) obtained for the same organic molecules on smooth reflecting surfaces of tin and silver.

## **DEDICATION**

This work is dedicated to those whose near infinite patience makes all things possible.... in time.

## ACKNOWLEDGEMENTS

I would like to acknowledge the following for their assistance in this thesis:

Dr. Ricardo Aroca, for years of patience, guidance, and imparting higher knowledge.

Mat Halls, for the high level calculations on 5,14-pentacenedione.

NSERC, for funding

and all those members of the Materials and Surface Science Group, at the University of Windsor, past and present:

Russ, Mat (again), Raymond, Alicia, Bob, Barry, Eric, Dorian, Santiago, Juncal, Roger, and others who have long since passed beyond the veil surrounding Windsor.

## TABLE OF CONTENTS

ABSTRACT	iii
DEDICATION	iv
ACKNOWLEDGEMENTS	v
LIST OF TABLES	vii
LIST OF FIGURES	viii
LIST OF ABBREVIATIONS	ix
CHAPTER	
I    INTRODUCTION	1
II   EXPERIMENTAL	7
III  VIBRATIONAL SPECTRA OF THE QUINONES	18
IV   SURFACE ENHANCED VIBRATIONAL SPECTROSCOPY	48
A  SURFACE ENHANCE RAMAN SPECTRA OF QUINONES	49
B  SURFACE ENHANCED INFRARED ON SILVER AND TIN SURFACES	54
CONCLUSIONS	65
APPENDIX A: PROPOSED VIBRATIONAL ASSIGNMENTS	66
APPENDIX B: SYNTHESIS OF 8,13-BENZO[A]NAPHTHACENEDIONE AND 7-METHYL-8,13-BENZO[A]NAPHTHACENEDIONE	84



## LIST OF TABLES

TABLE	PAGE	ABSTRACT
3.1	19	Group theory analysis of 5 quinones.
3.2	25	Q1 Observed Vibrational Assignment
3.3	31	Q2 Observed Vibrational Assignment
3.4	34	Q3 Observed Vibrational Assignment
3.5	36	Q5 Observed Vibrational Assignment
3.6	39	Q6 Observed Vibrational Assignment
3.7	41	Vibrational characteristic frequencies of the quinones.
3.8	42	Calculated vibrational spectrum of Q2 at HF/6-311G* level of theory.
4.1	58	Internal coordinate assignments for selected infrared wavenumbers of Q2.
A1.1 to A1.5	Appendix 1	Proposed vibrational assignments for the 5 molecules

## LIST OF FIGURES

FIGURE	PAGE	ABSTRACT
1.1	3	Schematic of 5 quinones studied
2.2	9	Evaporation system
2.3	12	TEM of 18nm tin film
2.4	13	Schematic of Potential Energy Surface
2.5	15	UV-VIS absorption spectra in solution
2.6	16	Electronic emission spectra in solution
3.0	20	Q2 Group Theory Analysis
3.1	23	Vibrational spectra of Q1
3.2	27	Computed molecular geometry at the MP2/6-31G* level
3.3	30	Vibrational spectra of Q2
3.4	33	Vibrational spectra of Q3
3.5	36	Vibrational spectra of Q5
3.6	38	Vibrational spectra of Q6
4.1	50	UV-VIS of 6nm Ag islands film
4.2	52	SERS and FT-Raman of Q2
4.3	53	FT-Raman and FT-SERS of Q6
4.4	57	SEIR of Q2 of 18nm Sn and 15nm Sn
4.5	59	SEIR and FT-IR of Q2
4.6	61	SEIR and RAIRS of Q2 on Sn
4.7	62	SEIR of Q2 on Sn and Ag

## LIST OF ABBREVIATIONS

Q1	1,4-anthracenedione
Q2	5,14-pentacenedione
Q3	6,15-hexacenedione
Q5	8,13-benzo[a]naphthacenedione
Q6	7-methyl-8,13-benzo[a]naphthacenedione
SEVS	Surface-enhanced vibrational spectroscopy
SEIR	Surface-enhanced infrared spectroscopy
SERS	Surface-enhance Raman scattering
AM1	Austin method 1
PM3	Parametric method 3
LCAO	Linear combination of atomic orbitals
SCF	Self-consistent field theory
LB	Langmuir-Blodgett
IR	infrared
UV	ultraviolet
$\alpha$	polarizability
$\mu$	dipole moment

## Introduction

The objective of the present work was to study the vibrational spectra of a series of molecular solids from the family of aromatic quinones. It is well known [1-3] that fundamental vibrational modes are **the spectroscopic observables** that provide information about the molecular ground state (or any excited state), chemical bonding, functional groups, *intra* and *inter* molecular interactions. There are several well established analytical techniques of VIBRATIONAL SPECTROSCOPY to carry out the experimental work in the gas, liquid and solid phases [1,2]. In the last twenty years, a new branch of vibrational spectroscopy has flourished: SURFACE ENHANCED VIBRATIONAL SPECTROSCOPY (SEVS) [3-6] where the subject of investigation are molecules adsorbed onto rough enhancing surfaces and interfaces. The most common and practical techniques to obtain complete vibrational information are the complementary **Infrared** and **Raman** spectroscopy. The discovery of the **surface-enhanced** Raman scattering effect (SERS [4], 1974-1977) and the realization that the electromagnetic enhancement [see, for instance, reviews 5 & 6] can also be achieved in the infrared region [7-9] of the spectrum has opened the gates in vibrational spectroscopy for analysis at the **nano, pico, and femto gram regime and possibly single molecule detection**.

At present, SERS is a well established analytical technique applicable to surface chemistry. Using SERS it is possible to determine the identity, bonding and orientation of adsorbed molecules. From the point of view of chemical analysis, the most striking aspect of SERS is its high *sensitivity* and *selectivity*. At the same time, SERS is operative at solid/gas, solid/liquid and solid/solid interfaces. The most common metal surfaces for SERS operation are Ag, Au, Cu, In, Ga and the alkali metals. At the present time, surface-enhanced infrared (SEIR) is still under development and at least one of our contributions to the area is described in this thesis.

The basic electromagnetic enhancement of the analytical signal in SERS and SEIR is dependent upon: i) the optical properties of the metal substrate ii) the shape of the metal particles or periodic surface iii) the size of the metal roughness or metal particle and the iv) the packing of the metal particles. It is evident that for the development of a highly efficient SERS surface, it is necessary to fabricate metallic surfaces where the radiative plasmon emission is maximized. The search for a universal enhancing-surface has been an aspiration that has been partially fulfilled. It could be said that rough Ag and Au surfaces are universal enhancing substrates. However, the search for the most efficient surface is ongoing.

As one of the main results of the present work, we describe the development of a new enhancing-surface for analytical applications in the area of SEIR. This surface is fabricated onto an infrared transparent substrate by evaporating 18 nm mass thickness of Sn. The investigation of semimetals and semiconductors for SEIR applications will be assisted by our discovery.

The thesis begins with the study of the vibrational characteristics of the quinones, as this information provides a fingerprint of the structure of the molecule. Fingerprints of smaller well defined molecules are commonly used to aid in the characterization of larger more complex systems consisting, in part, of these smaller units. Therefore, the study of the smaller systems, which can be modeled in great detail, can be used to predict characteristic spectral features of the larger quinones systems.

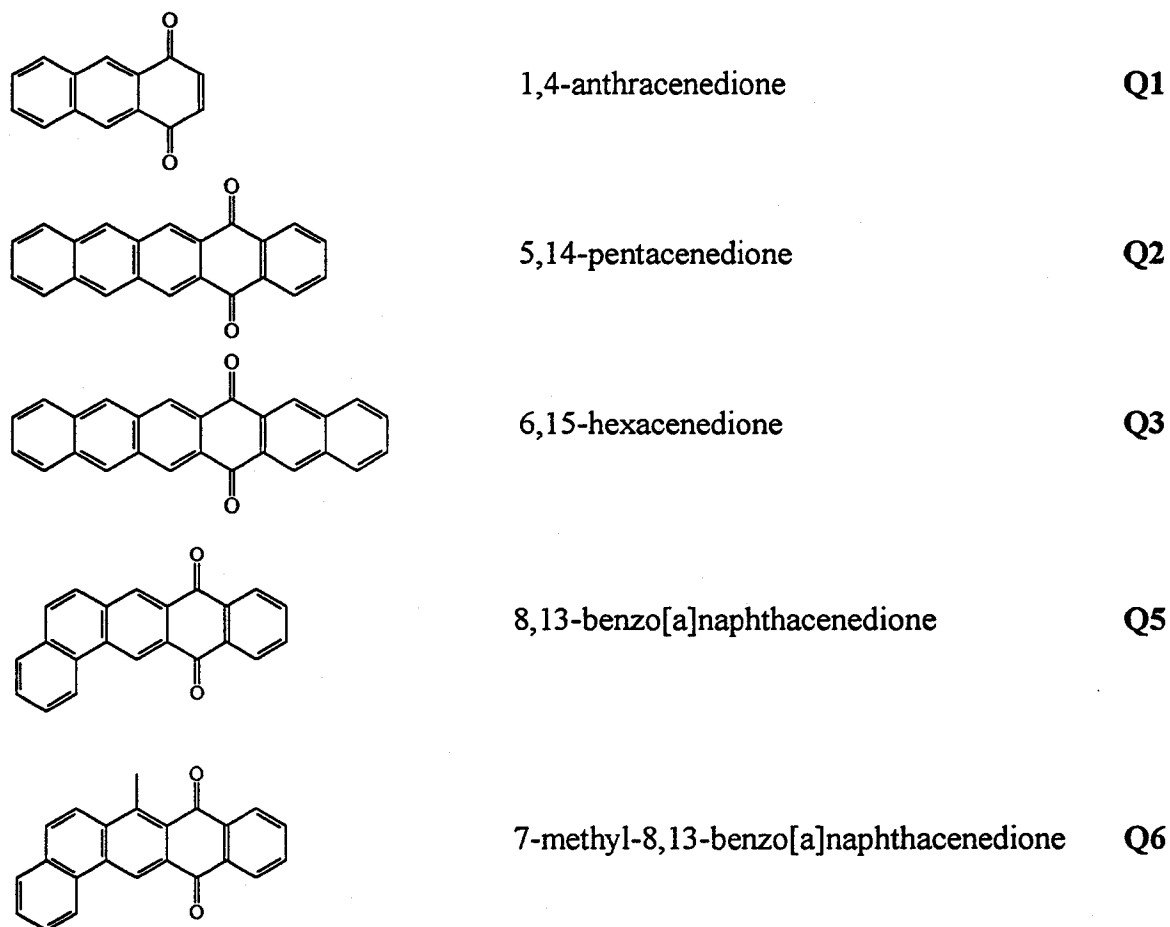
The series of quinones that have been studied are listed and shown in Figure 1.1.

Over the years quinones have gained increasing notoriety as they form the basis for a number of biological systems. Two well studied biological systems that contain the quinone group are ubiquinone (coenzyme Q) and vitamin K. A CIBA foundation symposium [10] was held to discuss these molecules and the role that they held in the electron transport mechanisms of biological processes. They also have chemical properties that have attracted the attention of scientists in the fields

of electrochemistry and photochemistry [11]. The smallest quinones, 1,4-benzoquinone, 1,4-naphthaquinone have been characterized extensively [12,13] and vibrational reports have been published for 1,4-anthracenedione [14] and longer linear symmetric quinones, 9,10-anthracenedione [15,17] , and 6,13-pentacenedione [18].

**FIGURE 1.1**

**5 QUINONES STUDIED**



Quinones are found in a variety of systems and are studied over a wide range of disciplines in science. The biological aspects of quinones have developed great interest as a number of important enzymes and molecules (vitamin K) contain a quinone molecule or molecules as a nucleus of the system. The properties of

quinones, mainly their role in electron transport, can provide a key to understanding the mechanism of certain fundamental biological processes. It is also the electron transport properties of quinones that drives much of the physical chemistry studies of these molecules.

In this study, the aptitude of the series of quinones for the formation of thin solid films has been investigated. It was found that evaporated films may easily be obtained for all the molecules, and ordered LB films have been obtained for all but 1,4-anthracenedione and 5,14-pentacenedione. The combination of these two properties, electron transport and thin film preparation, provides for the possibility of using these molecules in the development of chemical sensors.

The vibrational literature contains detailed studies of only the smallest quinone of the series. Calculations and vibrational assignments for the in-plane vibrations have been reported for 1,4-anthracenedione by Strokach *et al.* [14]. Singh & Singh [16] did a complete vibrational characterization of 1,4-naphthacenedione and 9,10-anthracenedione obtaining the infrared spectra in solution and solid phase and also with nujol mull. In their analysis of 1,4-anthracenedione the authors utilized previously published vibrational assignments for naphthalene and parabenzoquinone. Of the molecules in this study there are no vibrational data published on the 5,14-pentacenedione or the 6,15-hexacenedione. 8,13-benzo[a]naphthacenedione, 7-methyl-8,13-benzo[a]naphthacenedione and are novel and no literature references have been found for them.

## References - Chapter 1

1. E. Bright Wilson, J.C. Decius, P.C. Cross, *Molecular Vibrations*; Dover: New York, (1955) p1.
2. J.C. Decius, R.M. Hexter, *Molecular Vibrations in Crystals*, McGraw-Hill Int., New York, (1977).
3. J.J. Laserna, Editor, *Modern Techniques in Raman Spectroscopy*, John Wiley & Sons, Chichester, New York, (1996).
4. R.K. Chang, T.E. Furtak, Eds. *Surface Enhanced Raman Scattering*; Plenum: New York, (1982).
5. M. Moskovits, *Rev. Mod. Phys.* **1985**, *57*, 783.
6. R. Aroca, G.J. Kovacs in *Surface Enhanced Raman Spectroscopy in Vibrational Spectra and Structure*, (J.R. Durig ed.), Elsevier, Amsterdam, (1991), p55.
7. A. Harstein, J.R. Kirtley, J.C. Tang, *Phys. Rev. Letters*, **1980**, *45*, 201.
8. Y. Nishikawa, K. Fujiwara, K. Ataka, M. Osawa, *Anal. Chem.* **1993**, *65*, 556.
9. E. Johnson, Ph.D. Thesis. University of Windsor (1994).
10. G.E.W. Wolstenholme, C.M. O'Connor, Eds. *Quinones in Electron Transport, CIBA Foundation Symposium*, Little Brown and Co. Boston
11. G.J. Gleicher in *The Chemistry of the Quinoid Compounds, Part 1* S. Patai Ed. Wiley, London, (1974).
12. B. Lunelli, C. Pecile. *Spectrochimica Acta*, **1973**, *29A*, 1989.
13. N.S. Strokach, D.N. Shigorin. *Russ. J. Phys. Chem.* **1977**, *51*, 1774.
14. N.S. Strokach, T.V. Kainkova, D.N. Shigorin. *Russ J. Phys. Chem.* **1986**, *60*, 63.
15. A. Girlando, D. Ragazzon, C. Pecile. *Spectrochimica Acta* **1980**, *36A*, 1053.
16. S.N. Singh, R.S. Singh. *Spectrochimica Acta*, **1968**, *24A*, 1591.
17. K.K. Lehmann, J. Smolarok, O.S. Khalil, L. Goodman, *J. Phys. Chem.* **1979**, *83*, 1200.



18. L.P. Brivina, N.S.Strokach, D.N.Shigorin. *Russ.J.Phys.Chem.* **1981**, *55*, 1435.

## **Chapter 2: Experimental**

### **Synthesis**

The synthesis of the materials used in this thesis was carried out by Dr. P. Dibble. The description of the synthetic work for 8,13-benzo[a]naphthacenedione and 7-methyl-8,13-benzo[a]naphthacenedione has been included with his approval and can be found in Appendix B. Quinones 1,4-anthraquinone, 5,13-pentacenedione and 6,14-hexacenedione were prepared by a published procedure [1].

### **Preparation of Evaporated Films**

The evaporated films studied in this work were prepared in a vacuum evaporator comprised of a combination of commercial and in house components as illustrated in Figure 2.2. An Edwards E2M2 rotary vacuum pump was used as a forepump to an Edwards diffusion pump. These two pumps could attain a vacuum of the order of  $10^{-6}$  torr (1 torr = 133 Pa(Nm<sup>-2</sup>)). A jacket filled with liquid nitrogen was used to lower the pressure by an order of magnitude. Pressures in the system were measured using a Balzers TPR 010 Pirani gauge for pressures  $>10^{-3}$  torr and a Balzers IKR 020 cold cathode gauge for pressures  $<10^{-3}$  torr. Film thickness measurements were measured using a XTC Inficon quartz crystal oscillator which functions by measuring mass thickness. The crystal oscillator was also used to monitor the rate of evaporation.

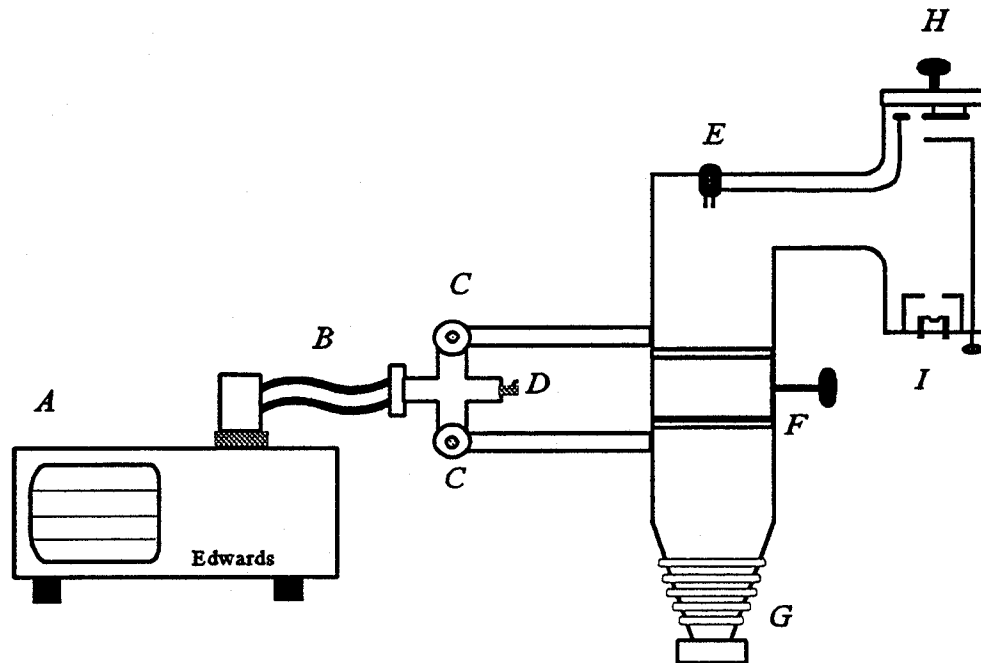
### **Metal Films**

Thin metal films for use in SEIR and SERS experiments were prepared using the metals Ag, Sn, and Au. The SEIR surfaces for use in transmission FTIR experiments were prepared by vacuum evaporation of the metals onto KBr disks, ZnS, and Ge substrates. Silver and gold films were evaporated to a mass thickness of 6 nm onto substrates held at a temperature of 200°C. Base pressure for the evaporation was  $4 \times 10^{-6}$  torr and the evaporation rate was maintained at 0.05 nm/s. The tin films were prepared to a mass thickness of 15 nm and 18 nm on substrates held at a temperature of 80°C. Evaporation rate and base pressure was maintained

as previously stated. The tin thin metal films were characterized using transmission electron microscopy. This was done in a JEOL 100CX TEM with 100 kV. TEMs of an 18 nm tin film recorded at 20k and 50k magnification are shown in Figure 2.2.

Smooth reflecting metal substrates used for RAIRS measurements were prepared by vacuum evaporation of 100nm mass thickness of Ag and 150 nm of Sn onto Corning 7095 glass slides. The substrates were maintained at temperatures of 200°C and 80°C respectively with a base pressure of  $4 \times 10^{-6}$  torr and an evaporation rate of 0.5 nm/s.

**FIGURE 2.2**  
**EVAPORATION SYSTEM**



- KEY:**
- A FOREPUMP
  - B HIGH VACUUM CONNECTOR HOSE
  - C VALVES
  - D PRESSURE RELEASE VALVE
  - E INSTRUMENTATION FEEDTHROUGH:  
HIGH PRESSURE GAUGE, DEPOSITION RATE GAUGE
  - F BUTTERFLY VALVE
  - G DIFFUSION PUMP
  - H LID: SUBSTRATE TABLE, THERMOCOUPLE AND  
HEATING ELEMENT FEEDTHROUGHS
  - I BASE: THERMOEVAPORATION POSTS, SOURCE BOAT,  
CONTROL FOR SUBSTRATE SHIELD

## **Organic Films**

Evaporation of the organic molecules in this work was performed in a twin system to the one described above for the evaporation of the metal films. In the case of the organic films the substrates used were maintained at ambient temperatures. The substrates to be used in RAIRS experiments were coated with a mass thickness of 40 nm of the organic molecules while transmission experiments utilized films of 10 nm to 15 nm mass thickness. In both the above cases the films were prepared at a base pressure of  $4 \times 10^{-6}$  torr and at an evaporation rate of 0.2 nm/s.

## **Infrared Spectroscopy**

All of the infrared spectra in this study were collected using a Bomem DA3 FT-IR spectrometer equipped with a liquid nitrogen cooled wide range MCT detector. The spectra were collected from the co-addition of 1024 scans with a sample box pressure of 5 torr. Infrared spectra of the bulk materials were collected through an isotropic dispersion in CsI from which pellets were formed. These spectra were collected with a spectral resolution of  $1 \text{ cm}^{-1}$ . SEIR transmission experiments were done under similar experimental collection conditions with a resolution of  $4 \text{ cm}^{-1}$ . Reflection infrared spectra were obtained using a Spectra-Tech variable angle reflectance accessory and an incidence angle of  $75^\circ$ .

## **Raman Spectroscopy**

Raman spectra were collected on a Bruker RFS100 FT-Raman microscope equipped with a Ge diode detector. The spectra were recorded with a  $2 \text{ cm}^{-1}$  resolution. All spectra were transferred to a PC computer and analyzed using Grams software available from Galactic Industries Corp.

## Theoretical analysis

In order to provide a basis for the computational calculations reported below a very brief summary of the theory behind these calculations is necessary. A good starting point for this discussion is the Schrödinger equation for stationary states of the form:

$$\hat{H}\Psi = E\Psi$$

where  $\Psi$  represents the wavefunction of the molecule.  $\hat{H}$  is a Hamiltonian operator which consists of kinetic and potential energy terms. Written explicitly we have:

$$\begin{aligned}\hat{H} &= T + V \\ &= -\hbar^2/2m(\nabla_{nn}^2 + \nabla_{ee}^2 + \nabla_{ne}^2) + V_{nn} + V_{ee} + V_{ne}\end{aligned}$$

where  $-\hbar^2/2m\nabla^2$  is the kinetic energy operator:  $(\partial^2/\partial x^2 + \partial^2/\partial y^2 + \partial^2/\partial z^2)$  and the subscripts n and e represent the nuclear and electronic coordinates respectively.

The Hamiltonian can be simplified by the Born-Oppenheimer approximation which allows for the separation of nuclear motion from electron motion thus the elimination of the  $\nabla_{ne}^2$  term from the aforementioned Hamiltonian.

The variational principle allows one to find an expectation for computational work. The energy is found using the complex conjugate of the wavefunction and integrating over all coordinates:

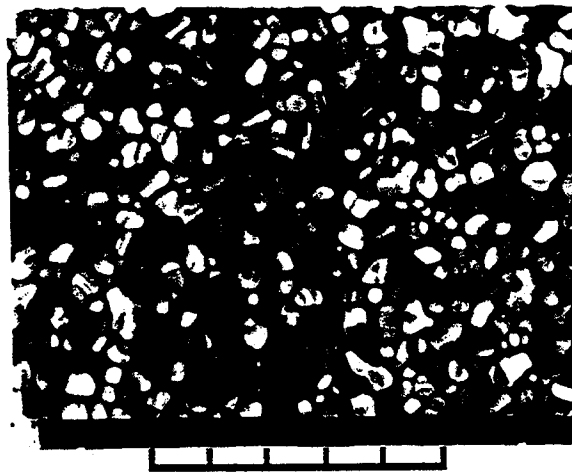
$$E_a = \int \Psi^* H \Psi d\tau / \int \Psi^* \Psi d\tau$$

The variational principle states that as the trial wave function  $\Psi$  comes closer to the true wave function for the lowest state of a given symmetry the energy,  $E_a$ , will decrease. Thus the true energy of the system can be represented as  $E_t \leq E_a$ .

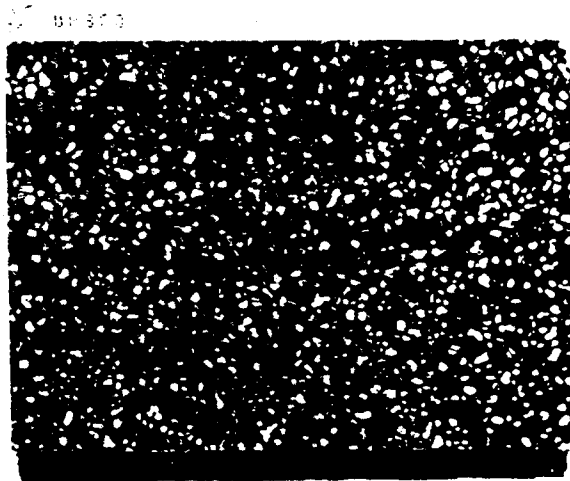
Computational calculations of these systems were done in two stages. The first stage involves a geometric optimization of the system. If the potential

Figure 2.3

TEM of 18nm Tin film



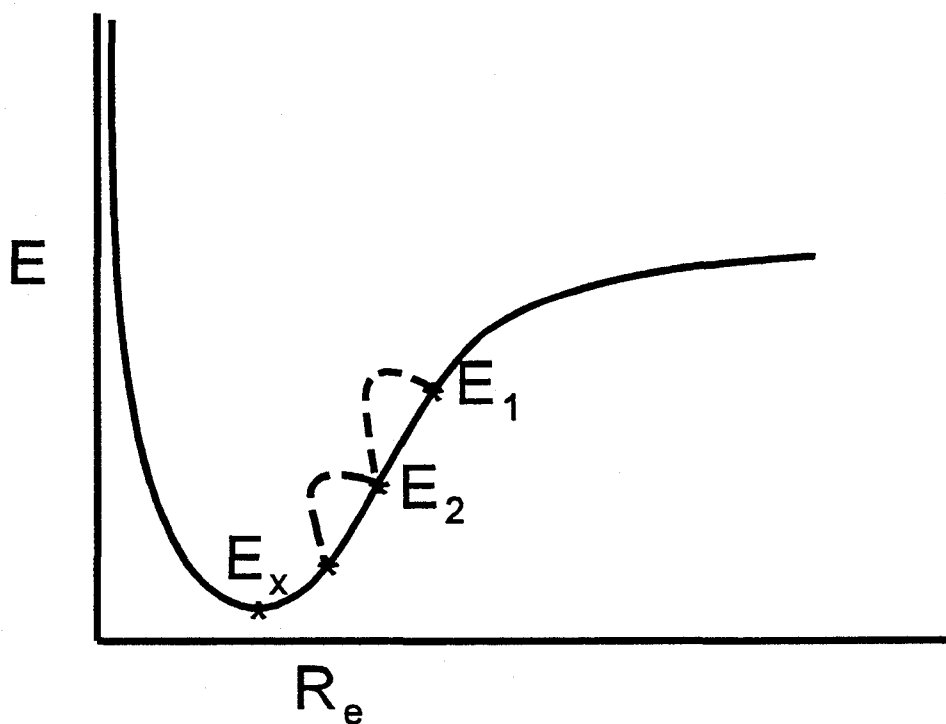
1 μm



2.5 μm

energy of two nuclei is plotted as a function of the distance between the two nuclei, a potential energy surface, Figure 2.4, can be obtained. Starting at an arbitrary point  $E_1$ , corresponding to the input geometry, a calculation of the gradient is performed ( $\partial E/\partial R$ ). The  $R$  is iteratively changed until the gradient is equal to zero, indicative of a minimum energy ( $E_x$ ) in the system. For a polyatomic system this calculation is carried out for each internal coordinate until the entire system is at an equilibrium geometry.

**Figure 2.4**  
**Schematic of a Potential Energy Surface**



Once a minimum energy for the molecule has been found the harmonic normal frequencies can be obtained for the molecular system. Starting with the general Hamiltonian:

$$H = \left\{ \sum_i (-\frac{1}{2} \nabla_i^2) - \sum_{i\mu} Z_\mu / r_{i\mu} + \sum_{i<j} 1/r_{ij} \right\}$$



where  $i$  and  $j$  are electronic indices and  $\mu$  is a nuclear index. The wave function  $\Psi$  is expressed as a linear combination of atomic orbitals (LCAO) [2].

Solving for the orbitals will yield Slater type orbitals, which are Lorentzian = in shape. This is correct for the exact solution of the hydrogen atom.

Unfortunately from a computational view Lorentzian orbitals are difficult to calculate. To remedy this the Lorentzian orbitals are approximated as a linear combination of Gaussian orbitals.

$$\phi_i = \sum_k c_{ik} \chi_k$$

where  $\phi$  represents the molecular orbital and  $\chi$  the atomic orbital.

Using a large basis set of these Gaussian orbitals one can obtain a close approximation to the true Lorentzian orbital and Gaussian orbitals have the inherent property that a product of two Gaussians will result in another Gaussian.

$$E(x)|_0 = E(0) + [\partial E/\partial x]\delta x + 1/2[\partial^2 E/\partial^2 x]\delta^2 x$$

At a minimum  $\partial E/\partial x=0$

From self consistent field theory (SCF) [3],  $E(0)$  is known so the force constants can be calculated. The force constants which are composed into a force constant matrix. This matrix is then transformed into mass weighted cartesian then diagonalized to yield frequencies and normal mode displacement vectors.

Utilizing the Hartree-Fock equations one can iteratively reach the best Slater-determinant. For a self consistent field this allows for the following:

$$H^{SCF} \phi_i = \epsilon_i^{SCF} \phi_i$$

From this the eigenvalues of the orbitals  $\epsilon_i$  can be obtained which are directly correlated to the orbital energies. From these energies the force constant for the vibration,  $k$ , can be obtained. Given the force constant of the vibration and the reduced mass of the normal mode components of the vibration the frequency

can be calculated.

$$\hat{U} = (k/\mu)^{1/2}$$

Semi-empirical calculations were performed on a Pentium Pro 200 PC using Hyperchem 4.0. Calculations involved geometry optimization followed by harmonic frequency calculations for each of the molecules using two semi-empirical theoretical methods: Austin Method 1 (AM1) [4] and Parametric Method 3 (PM3) [5]. Calculations for Q2 were also done using MP2/6-31G\* and HF/6-311G\* basis sets with Gaussian 94 software [6].

The electronic absorption spectra are included below as an analytical identification in the study of the quinones. The UV-vis absorption and electronic emission spectra for the series of quinones has been obtained in solution and is presented in Figures 2.5, 2.6.

**FIGURE 2.5**  
**UV-vis absorption in solution**

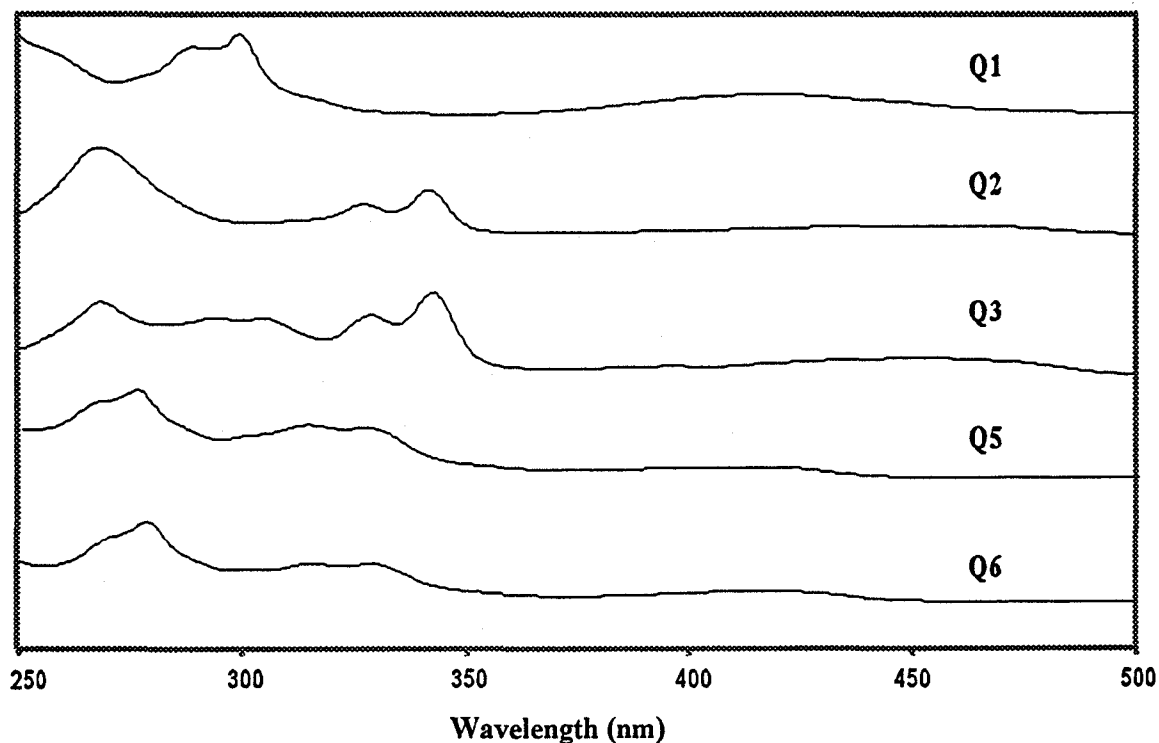
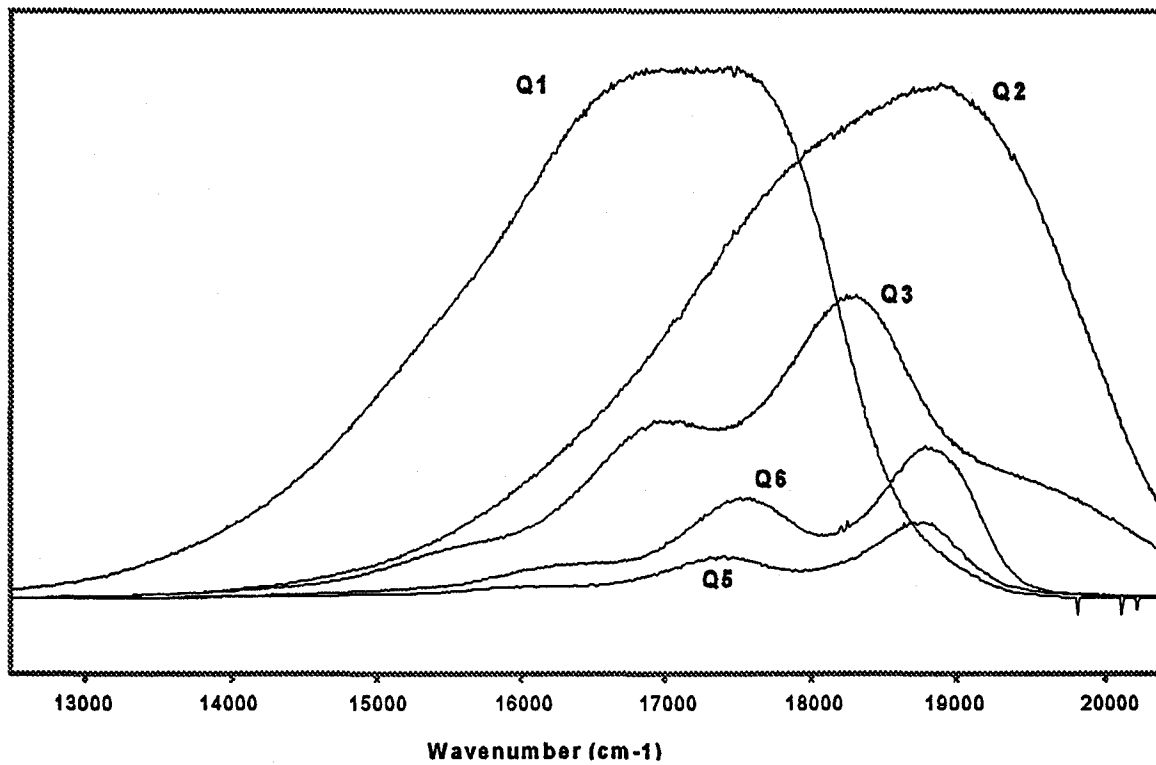


**FIGURE 2.6**  
**Electronic emission in solution**



## REFERENCES

- 1 James G. Smith, Peter W. Dibble and Richard E. Sandborn, *J. Org. Chem.* **1986**, *51*, 3762.
- 2 W.G. Richards, J.A. Horsley; *Ab Initio Molecular Orbital Calculations for Chemists*, Claredon Press, Oxford, (1970), p15.
- 3 W.G. Richards, J.A. Horsley; *Ab Initio Molecular Orbital Calculations for Chemists*, Claredon Press, Oxford, (1970), p47.
- 4 M.J. Dewar, E.G. Zoebish, E.F. Healy. *J.Am.Chem.Soc.***1985**, *107*, 3902.
- 5 J.J.P. Stewart. *J. Comput. Chem.* **1989**, *10*, 209.
- 6 *Gaussian 94*, Revision C.3, M.J. Frisch, G.W. Trucks, H.B. Schlegel, P. M.W. Gill, B.G. Johnson, M.A. Robb, J.R. Cheeseman, T. Keith, G.A. Petersson, J.A. Montgomery, K. Raghavachari, M.A. Al-Laham, V.G. Zakrzewski, J.V. Ortiz, J.B. Foresman, J. Cioslowski, B.B. Stefanov, A. Nanayakkara, M. Challacombe, C.Y. Peng, P.Y. Ayala, W. Chen, M.W. Wong, J.L. Andres, E.S. Replogle, R. Gomperts, R.L. Martin, D.J. Fox, J. S. Binkley, D.J. Defrees, J. Baker, J.P. Stewart, M. Head-Gordon, C. Gonzalez, and J.A. Pople, Gaussian, Inc., Pittsburgh PA, (1995).

## Chapter 3

### Vibrational spectra of the quinones.

The vibrational spectra of a series of five aromatic quinones are discussed: 1,4-anthracenedione, [Q1], 5,14-pentacenedione, [Q2], 6,15-hexacenedione, [Q3], and the two novel compounds: 8,13-benzo[a]naphthacenedione, [Q5], and 7-methyl-8,13-benzo[a]naphthacenedione, [Q6]. Of these five compounds the vibrational spectra of 1,4-anthracenedione, has been previously reported [1]. For the remainder of the molecules, the FT-Raman and FT-IR are being reported here for the first time. These molecules form the nucleus of a number of dye derivatives and can be used as a model systems for the study of these more complex molecules.

Vibrational studies are now commonly assisted by the calculation of theoretical harmonic fundamentals, atomic displacement representations, and spectral intensities. These calculations are carried out here using Hartree-Fock based semi-empirical methods. Two semi-empirical methods are commonly used AM1 and PM3. The relative performance of these two methods is well known [see review 3]. Here we present the result of calculations of fundamental vibrations of this series of aromatic quinones using the semi-empirical methods AM1 and PM3, as an assistance to the assignment of the observed fundamental vibrational frequencies of these molecules.

There are  $3N-6$  normal modes for a non-linear polyatomic molecule. The assignment of vibrational fundamentals is facilitated by the application of group theory given the symmetry point group of the molecular system. Of the five molecules in this study, three of them, Q1, Q2, Q3 belong to the  $C_{2v}$  symmetry point group. They have a 2-fold rotational axis in addition to two molecular planes as symmetry elements. Q5 can be classified as belonging to the  $C_s$  point group having only a molecular plane as a symmetry element. And the molecule of Q6 is of  $C_1$  symmetry, i.e., it has no symmetry elements, except E. Q6 could have been assigned as  $C_s$  symmetry if the methyl substituent group were fixed in such a way

as to conserve the symmetry of the molecular plane in Q5 but this assignment was rejected as the computational calculation of the equilibrium geometries of this molecule did not result in this conformation. The total irreducible representation obtained from the group theory analysis for each molecule is summarized in Table 3.1.

**TABLE 3.1**

	Symmetry Point Group	Irreducible Representations	IR Active Modes	Raman Active Modes	# of Stretching Vib.	# of In Plane Bends	# of Out of Plane Vib.
Q1	$C_{2v}$	$23a_1 + 11a_2 + 10b_1 + 22b_2$	$22a_1 + 10b_1 + 22b_2$	all	26	19	21
Q2	$C_{2v}$	$35a_1 + 17a_2 + 16b_1 + 34b_2$	$35a_1 + 16b_1 + 34b_2$	all	40	29	33
Q3	$C_{2v}$	$41a_1 + 20a_2 + 19b_1 + 40b_2$	$41a_1 + 19b_1 + 40b_2$	all	47	34	39
Q5	$C_s$	$69a' + 33a''$	all	all	40	29	33
Q6	$C_1$	111a	all	all	43	n/a	n/a

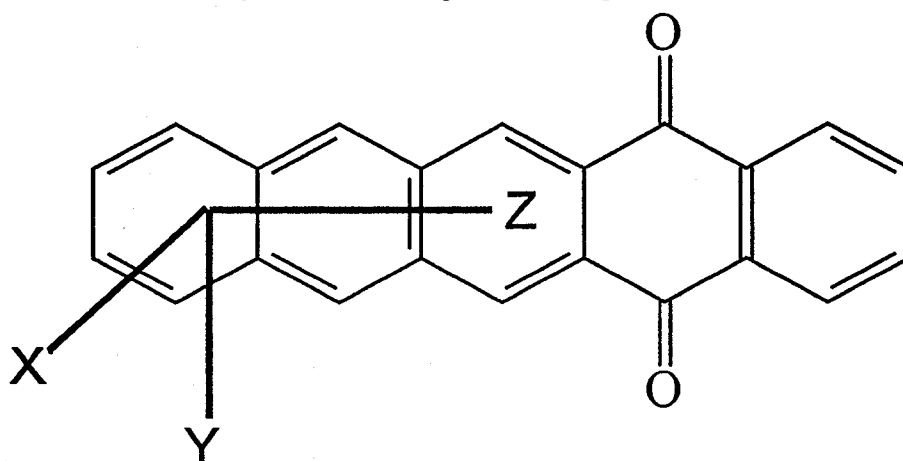
To illustrate the calculation of the modes in each symmetry species shown in the table, a detail examination of Q2 is done as an example. Q2 contains 36 atoms and thus, by  $3N-6$ , 102 vibrational modes. To calculate the number of stretching modes we use the formula:

$$N-1+f$$

where  $f$  is the number of rings in the system and  $N$  is the total number of atoms. Therefore we have  $(36-1+5)$  40 stretching vibrations. Of the remaining 62 modes 29 are in-plane bends and 33 are out-of-plane modes. To obtain the total reducible representations for this system the effect of the symmetry operations on these modes is examined. The point group  $C_{2v}$  contains four symmetry elements: E,  $C_2$ ,

$\sigma_{xz}$ , and  $\sigma_{yz}$ . Figure 3.0 shows a molecule of Q2 aligned along the Cartesian coordinates and a reproduction of a character table for the  $C_{2v}$  point group [2]. The vibrational representation has been added to the character table as shown in Figure 3.0.

**Figure 3.0**  
**Q2 Group Theory Analysis**



$C_{2v}$	E	$C_{2(z)}$	$\sigma_{xz}$	$\sigma_{yz}$
$a_1$	1	1	1	1
$a_2$	1	1	-1	-1
$b_1$	1	-1	1	-1
$b_2$	1	-1	-1	1
$\chi_v$	102	2	0	36
n	36	0	0	36

To calculate the number of modes in each of the symmetry species the following reduction formula may be applied:

$$a_i = 1/h \sum g_R X_{i(R)} X_{V(R)}$$

where  $a_i$  is the number of times that the irreducible representation  $i$  occurs in the reducible representation.

$h$  is the order of the group

$X_{i(R)}$  character of the symmetry species under an operation  $R$

$X_{V(R)}$  character of the reducible representation under an operation  $R$

$g_R$  number of operations in the class

For example taking the group  $b_2$  :

$$b_2 = 1/4(102*(1) + 2*(-1) + 0*(-1) + 36*(1)) = 34$$

Repeating this for all the groups we get the total irreducible representations for Q2 to be:

$$35a_1 + 17a_2 + 16b_1 + 34b_2.$$

The calculated optical parameters are the dipole moment derivatives  $(\partial\mu/\partial Q_i)$  in the series:

$$\mu = \mu_o + (\partial\mu/\partial Q_i)\delta Q_i + (\partial\mu^2/\partial Q_i\partial Q_j)\delta Q_i\delta Q_j + \dots$$

Where  $\mu_o$  is the equilibrium dipole moment, and  $\delta Q_i$  represents the infinitesimal variation of the internal coordinate  $Q_i$ . The nonlinear terms are neglected within the electric harmonic approximation.

A standard absorption relation, Beer's Law, can be rearranged so that the molar absorptivity is isolated to one side of the equation. It is this species that is calculated for in the computational methods. Thus it is the intensity of band integrated over the width of the band that is reported in the calculations and in the



tables below. The calculated infrared intensities are reported in  $\text{km mol}^{-1}$ , units that are related to the integrated absorption intensity of an infrared transition:

$$A_s = \frac{1}{cl} \int_{band} \ln\left(\frac{I_o}{I}\right) dv$$

where  $c$  is the concentration in moles litre<sup>-1</sup> ( $\text{mmol/cm}^3$ ),  $l$  is the pathlength in cm and  $dv$  is in  $\text{cm}^{-1}$ ,  $A$  is given in  $\text{cm mmol}^{-1}$  (unit called DARKS). The value in darks divided by 100 is the value of  $A$  in  $\text{km mol}^{-1}$ . In units of  $\text{km mol}^{-1}$  a strong absorption is of the order of 1000 and a weak absorption is  $0.1 \text{ km mol}^{-1}$ . For gases where the concentrations are given in terms of pressure then

$$A/(\text{km mol}^{-1}) = RT (A/\text{cm}^2 \text{atm}^{-1})$$

$R = 82.05 \text{ cm}^3 \text{atm}^{-1}$  and  $T$  is temperature in K degrees.

The conversion factor from  $\text{cm}^2 \text{atm}^{-1}$  to darks is 22.415. For example a typical integrated absorption of  $500 \text{ cm}^2 \text{atm}^{-1}$  translate into a total value of 11207 darks.

## ASSIGNMENT OF OBSERVED VIBRATIONAL SPECTRA

### Vibrational spectra of 1,4-anthracenedione, [Q1]

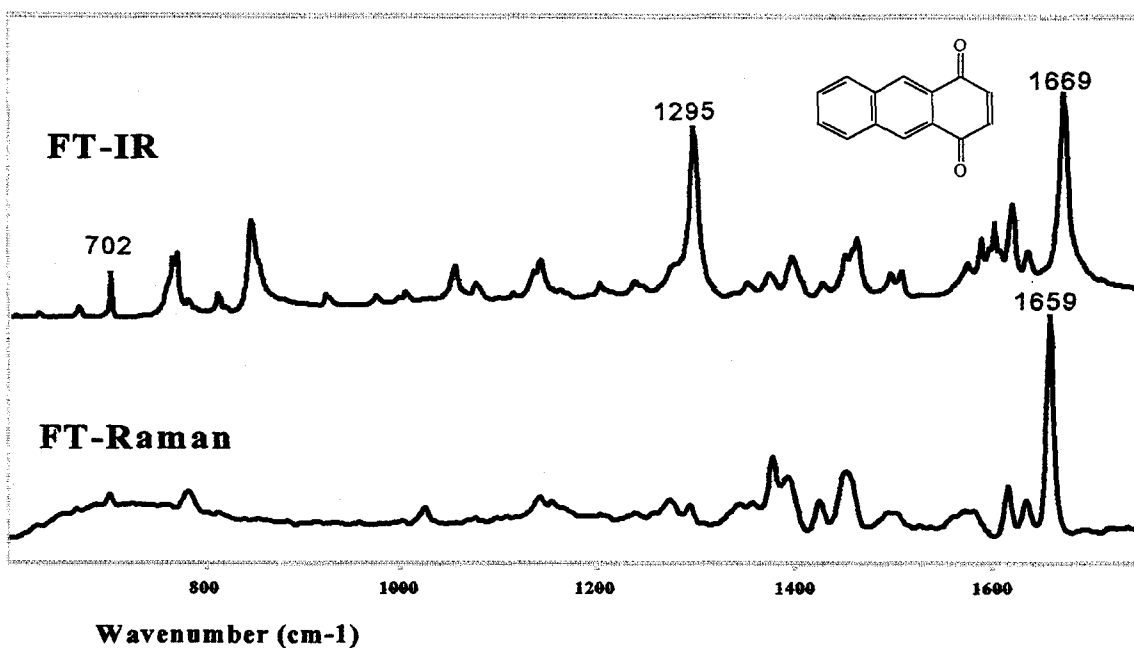
The FT-Raman and infrared spectra of the 1,4-anthracenedione, [Q1] aromatic quinone are shown in Figure 3.1. The calculated frequencies, experimental wavenumbers, symmetry of vibration, and proposed assignments for each observed vibrational band are listed in Table A1.1 of the Appendix 1.

When using a semi-empirical Hartree-Fock based method to calculate theoretical normal mode vibrations empirical scaling factors are often employed to bring the calculated frequencies closer to the experimentally observed frequencies. The scaling factor is needed since calculations always overestimating the true energy of the system,  $E_{\text{calc}} > E_{\text{actual}}$ . This error is due to the neglecting of anharmonicity and correlational effects. In this work the theoretical calculated frequencies were corrected with a homogeneous scaling factor [3] of 0.9.

However, the 0.9 scaling factor introduces a significant error for the C-H stretching modes. Therefore, the C-H stretching modes were scaled using a 0.95 factor.

**Figure 3.1**

**1,4-ANTHRACENEDIONE (Q1)**



A Normal Coordinate analysis of in-plane  $23 a_1$  and  $22 b_2$  modes was reported by Strokach et al. [1]. It seems adequate to discuss the assignment of observed vibrational modes following the separation of in-plane and out-of-plane modes. Since the out-of-plane modes are distinct by symmetry, we will discuss them as a group, while we will divide the in-plane modes according to the internal coordinates.

C=O group vibrations

The two carbonyl groups are clearly observed in the vibrational spectra. The antisymmetric stretching vibration provides the greatest change in the dipole moment and is thus observed as a very strong band in the infrared spectrum at  $1669 \text{ cm}^{-1}$ . The corresponding symmetric stretching mode of this group produces

a strong band in the Raman spectra observed at  $1659\text{ cm}^{-1}$ . As it is frequently seen in symmetric and antisymmetric stretching vibrational modes, the symmetric mode occurs at a lower energy than the antisymmetric mode. Notably, the quantum mechanical computation predicts the opposite trend, and it is also different from what has been reported for the symmetric 9,10-anthracenedione [4].

#### C-C ring stretching vibrations

The C-C ring stretching modes can be found between  $1240$  and  $1650\text{ cm}^{-1}$ . Strong modes are observed in the Raman at  $1452\text{ cm}^{-1}$ , for a ring stretching mode,  $1296\text{ cm}^{-1}$  for a ring breathing mode and at  $1240\text{ cm}^{-1}$  for an in plane ring deformation. In the infrared strong bands observed at  $1372\text{ cm}^{-1}$  and  $1294\text{ cm}^{-1}$  are assigned as in plane ring stretching modes. The ring stretching mode, at  $1294\text{ cm}^{-1}$ , is the second strongest band observable in the spectrum of 1,4-anthracenedione. As the number of aromatic rings in the system is increased this band increases in intensity becoming stronger than the carbonyl stretching band.

#### C-H bending vibrations

In the spectrum on Q1 only a few of the C-H bending vibrations are observed with any remarkable relative intensity. In the infrared spectrum the band observed at  $973\text{ cm}^{-1}$  is assigned to a C-H bending mode. In the Raman spectrum of Q1 no strong C-H bending vibrations are identified.

#### Out of plane vibrations

In the infrared spectrum of Q1 a few of the out of plane modes are clearly seen. In particular the bands at  $765\text{ cm}^{-1}$  and  $669\text{ cm}^{-1}$  we've assigned to out of plane ring deformation vibrations.

A summary for the vibrational assignment of the observed infrared and Raman bands is provided in table 3.2. This table consists of: the vibrational mode, as determined through computational methods; the calculated frequency of the mode; the x, y, and z components of the dipole moment derivatives of the vibration; the calculated intensity of the vibration; the symmetry of the vibration; the observed Raman and infrared bands and tentative assignments.

**Table 3.2****Q1 Observed Vibrational Assignment**

Mode	Frequency (scaled) (cm <sup>-1</sup> )	$\mu_y$ short axis	$\mu_z$ long axis	$\mu_x$ out of plane	Intensity (km/mol)	Symmetry	IR/Raman (cm <sup>-1</sup> )	Assignment
22	727	0	0	-1	20	b1	669	op ring bend
25	769	.3	.5	0	7	a1	702/704	ip ring stretch
26	818	0	0	-1.7	58	b1	765	op ring deformation
36	1044	.4	-.8	0	16	a1	973	ip H bend
43	1206	.4	.7	0	11	a1	1240	ip ring deformation
45	1263	1	2	0	104	a1	1294/ 1296	ip ring breathing
47	1323	.1	.1	0	13	b2	1372	ip ring deformation
51	1487	1	1.8	0	75	a1	1452	ip ring stretch
57	1831	2.9	1.6	0	202	b2	1668	C=O antisym
58	1834	.8	1.3	0	43	a1	1658	C=O sym

**Vibrational spectra of 5,14-pentacenedione [Q2]**

Vibrational analysis of 5,14-pentacenedione was done [5] using the HF/6-311G\* [6] level of theory. The results from these calculations are shown in Table 3.8. In the table the units for infrared intensity are given in km/mol, these are the SI units for IR intensity. The empirical analysis of Q2 is performed by examination of the strongest bands in the spectrum and comparing them with the predicted frequencies calculated from the computational methods. Comparison with

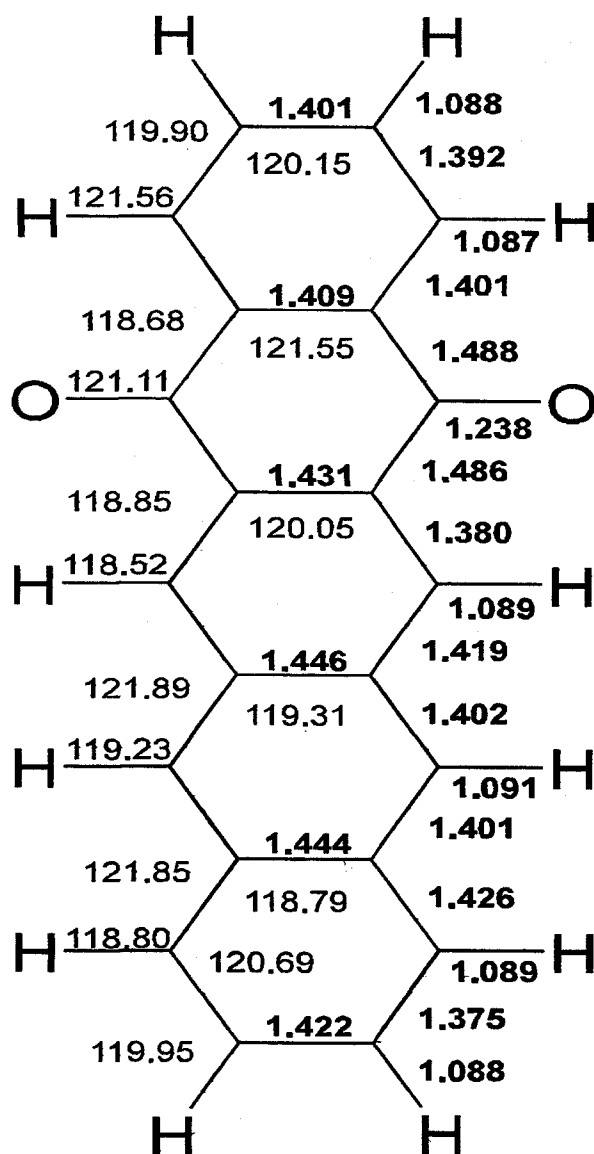
published literature for similar systems is also done.

Assignments of the vibrations of these molecules were made through the visualization of the atomic displacement representations that are obtained from theoretically calculated Raman and infrared spectra.

Higher level calculations [5] were also carried out for Q2 using a MP2/6-31G\*[6] basis set. The optimized geometry of the molecule Q2 at the MP2 level is shown in figure 3.2.

Figure 3.2

Computed molecular geometry at the MP2/6-31G\* level.



Bond lengths are in bold type and are reported in angstroms, bond angles are regular type and are given in degrees. With a  $C_{2v}$  symmetry the calculated geometrical parameters are mirrored across the  $\sigma_{xz}$  mirror plane. The molecule also conforms to a planar geometry.

In the calculations for Q2 we find a very intense band at  $1289\text{ cm}^{-1}$  (after scaling by 0.9). The third strongest band in the infrared intensity is calculated to be  $1267\text{ cm}^{-1}$ . Comparatively the infrared spectrum of Q2 (figure 3.3) contains two strong bands at  $1253\text{ cm}^{-1}$  and  $1294\text{ cm}^{-1}$  that are assigned to ring stretching ( $1294\text{ cm}^{-1}$ ) and a coupling of C-H bending and ring stretching modes at  $1253\text{ cm}^{-1}$ . The ring stretching mode is characteristic in all of the quinones studied with wavenumbers listed in table 3.7. In an early report Singh and Singh [3] identified a strong C-C stretching mode in 1,4-naphthaquinone at  $1295\text{ cm}^{-1}$  and a similar mode in 9,10-anthraquinone at  $1290\text{ cm}^{-1}$ .

There is a strong Raman band in the  $1400\text{ cm}^{-1}$  region that is in correspondence with the calculated value of  $1421\text{ cm}^{-1}$  for Q2. The HF calculations indicates that this ring stretching mode should be the strongest Raman band in the spectrum. Notably, this mode shows characteristic strong relative intensity for condensed aromatic molecules; but it is not prominent in the spectrum of 1,4-anthracenedione (Q1).

In the low frequency section of the mid-infrared spectrum vibrational modes are highly coupled and correspondingly less "characteristic" modes. However, the out-of-plane vibrations are of particular interest in this region. The HF computation produces a band at  $723\text{ cm}^{-1}$  (observed at  $709\text{ cm}^{-1}$ ) with a strong infrared intensity (the strongest in this spectral region). The observed band at  $709\text{ cm}^{-1}$  is a characteristic out-of-plane vibration with C=O wagging and C-H wagging contributions. A band of similar strong intensity was reported by Singh and Singh[5] and was also assigned to an out-of-plane wag. Similar bands are also observed in the other members of the series and are compiled in table 3.7

#### C=O group vibrations

In Q2 the carbonyl stretching vibrations are strong and distinctly observed in the infrared and Raman spectrum. In the infrared the antisymmetric stretching vibration is assigned as  $1667\text{ cm}^{-1}$ . The symmetric carbonyl stretching vibration is observed as a very intense band in the Raman at  $1659\text{ cm}^{-1}$ . In the infrared

spectrum the symmetric band can be seen only as a weak shoulder.

#### C-C ring stretching vibrations

The in plane ring stretching vibrations are more numerous and more intense in Q2 than the comparable bands found in Q1. In the Raman we assign the strong band at  $1418\text{ cm}^{-1}$  to a symmetric in plane ring stretching. Ring vibrations are also observable in the Raman at  $1341\text{ cm}^{-1}$ ,  $1250\text{ cm}^{-1}$ , and  $1204\text{ cm}^{-1}$ . In the infrared the strongest vibration is the ring stretching mode at  $1296\text{ cm}^{-1}$ . A combination ring deformation + CH bending mode found at  $1252\text{ cm}^{-1}$  is also very intense. Ring stretching vibrations are also observed at  $1344\text{ cm}^{-1}$  and  $1420\text{ cm}^{-1}$ . A weak band observed at  $1163\text{ cm}^{-1}$  has been assigned to a C-H bending and ring stretching vibration.

#### C-H bending vibrations

The vibrational mode that has the largest contribution from the CH bending is observed in the spectrum of Q2 at  $1004\text{ cm}^{-1}$  as a weak band in the Raman spectrum.

#### Out of plane vibrations

In the infrared an out of plane vibrational mode observed at  $866\text{ cm}^{-1}$  has been assigned to molecular deformation. Out of plane CH wagging modes are observable at  $759\text{ cm}^{-1}$  and  $709\text{ cm}^{-1}$  in the infrared and at  $760\text{ cm}^{-1}$  in the Raman.

A summary of the strongest bands observed in the vibrational spectra, infrared and Raman, of Q2 is given in table 3.3.



Figure 3.3

5,14-PENTACENEDIONE (Q2)

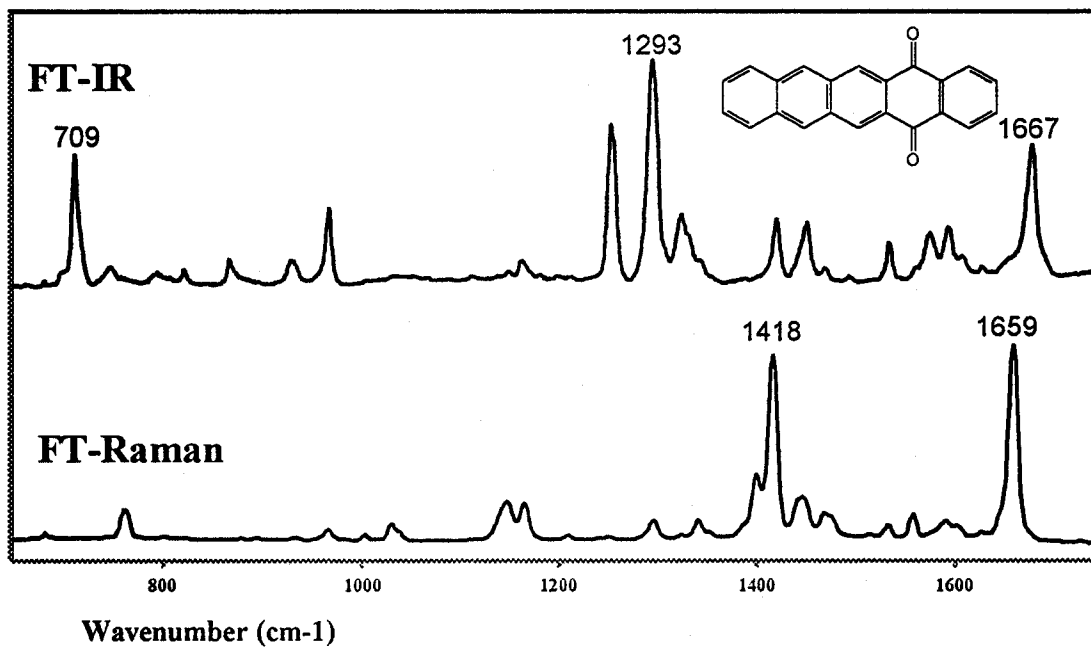


**Table 3.3**

**Q2 Observed Vibrational Assignment**

Mode	Fre- quency (scaled) (cm <sup>-1</sup> )	$\mu_y$ short axis	$\mu_z$ long axis	$\mu_x$ out of plane	Inten- sity (km /mol)	Sym- metry	IR/ Raman (cm <sup>-1</sup> )	Assignment
33	678	0	0	1.7	53	b1	678/ 678	CH wag
36	723	0	0	1.0	17	b1	709	CH wag
37	751	0	0	.8	11	b1	-/-	CH wag
41	825	0	0	.7	8	b1	759/ 760	CH wag
49	886	0	0	.9	15	b1	866	molecular deformation
53	921	.3	.6	0	8	b2	933 /933	molecular deformation
54	1025	.8	1.3	0	44	a1	-/-	molecular deformation
57	1066	.4	.7	0	14	a1	1004/ 1003	CH bend IP
64	1168	.2	.1	0	68	a1	1163	ring stretch
69	1249	.5	.9	0	20	a1	1212/ 1204	ring deformation
71	1296	.7	.4	0	13	b2	1252/ 1250	ring deformation + CH bend
72	1310	1.1	1.9	0	84	a1	1293/ 1296	ring breathing
74	1344	.9	1.6	0	66	a1	1344/ 1341	IP ring deformation
76	1434	.6	1.0	0	28	a1	1420/ 1418	ring deformation

83	1569	.4	.8	0	15	a1	1558	ring stretch
89	1818	2.6	1.5	0	165	b2	1667	C=O antisym stretch
90	1822	.6	.8	.1	23	a1	1658	C=O symmetric stretch

### 6.15-HEXACENEDIONE

The vibrational spectra of the nonsymmetric Q3 molecule is reported here for the first time.

#### C=O group vibrations

The antisymmetric carbonyl vibration is observed as the strongest band in the infrared spectrum of Q3 at 1675  $\text{cm}^{-1}$ . The complementary symmetric stretching vibration of the carbonyl is found at 1656  $\text{cm}^{-1}$ . The Raman band has a relatively low relative intensity compared to the C=O band in the other molecules studied in this work.

#### C-C ring stretching vibrations

Ring stretching vibrations can be observed from 1240  $\text{cm}^{-1}$  to 1650  $\text{cm}^{-1}$ . In the Infrared a very intense band can be observed at 1292  $\text{cm}^{-1}$  and is assigned to a ring stretching mode. The other intense modes observed at 1255  $\text{cm}^{-1}$  and 1200  $\text{cm}^{-1}$  are assigned to ring stretching coupled with CH bending modes. The most intense band found ca. 1500  $\text{cm}^{-1}$  is assigned to a C=C ring stretching vibration. The vibrational bands observed at 1393  $\text{cm}^{-1}$ , and 1418  $\text{cm}^{-1}$  are fairly intense in the infrared and very intense in the Raman. These bands are also assigned to in plane ring stretching vibrations.

#### C-H bending vibrations

One band in the Raman spectrum of Q3 has been assigned with a very large contribution from the CH bending vibration. It is observed at 1253  $\text{cm}^{-1}$  in the FT-

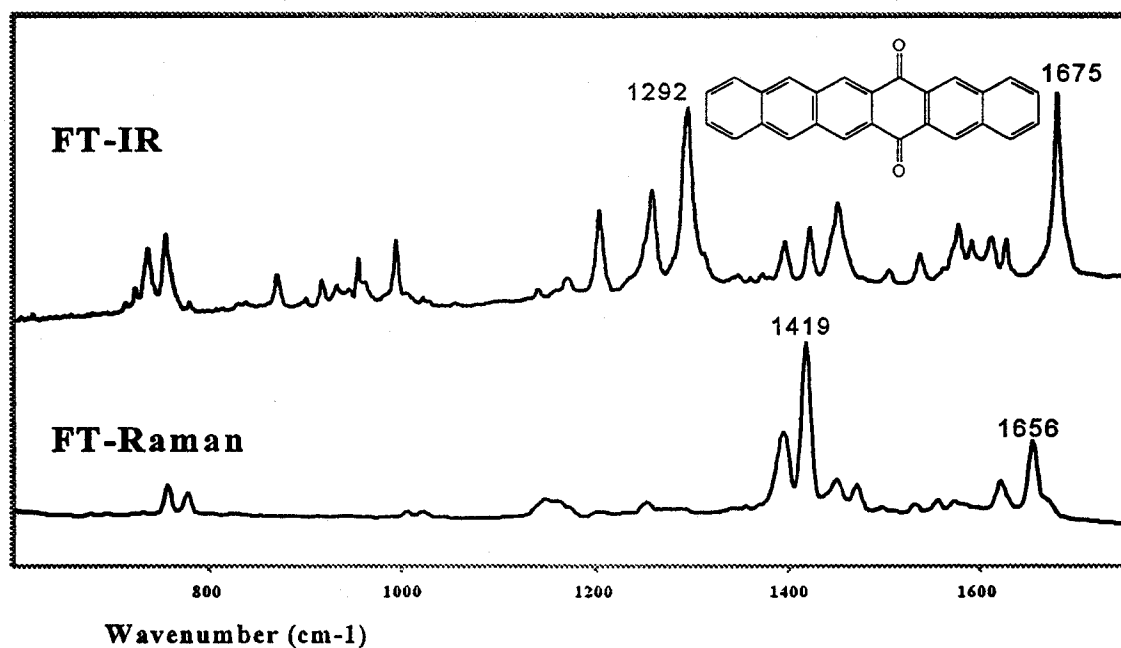
Raman spectrum.

### Out of plane vibrations

Below  $1000\text{ cm}^{-1}$  most of the observed bands arise from out of plane modes. In the infrared the two bands observed at  $912\text{ cm}^{-1}$  and  $778\text{ cm}^{-1}$  are assigned to CH wagging vibrations. The band at  $778\text{ cm}^{-1}$  is also observable in the Raman spectrum. Below  $750\text{ cm}^{-1}$  ring deformations become prominent. The bands observed at  $754\text{ cm}^{-1}$  and  $736\text{ cm}^{-1}$  in the infrared and  $755\text{ cm}^{-1}$  and  $734\text{ cm}^{-1}$  (weak) in the Raman are assigned to out of plane ring deformation modes.

**Figure 3.4**

### **6,15-HEXACENEDIONE (Q3)**



A summary of experimentally observed frequencies and tentative assignment for Q3 is offered in table 3.4

Table 3.4

## Q3 Observed Vibrational Assignment

Mode	Fre- quency (scaled) (cm <sup>-1</sup> )	$\mu_y$ short axis	$\mu_z$ long axis	$\mu_x$ out of plane	Inten- sity	Sym- metry	IR/ Raman (cm <sup>-1</sup> )	Assignment
21	419	0	0	0.9	14	b1	-/-	ring deformation
24	430	0.1	0.1	0.7	11	b1	-/-	ring deformation
40	684	0	0	0.9	15	b1	724/-	C=O bend
42	724	0	0	1.2	30	b1	736/ 734	ring deformation
44	732	0.2	0.3	1.0	22	b1	754/-	ring deformation
49	824	0	0	0.8	12	b1	778/ 779	CH wag
60	888	0.1	0.1	1.0	17	b1	912/ 912	CH wag
64	1030	0.8	1.4	0.2	49	a1	991	ring deformation IP
77	1178	1.2	2.1	0.1	112	a1	1253	CH bend
81	1247	1.3	2.3	0.4	129	a1	1292	CH bend
83	1289	0.8	0.5	0	16	b2	1310	ring stretch
86	1339	0.5	0.9	0	19	a1	1343/ 1342	CH bend
87	1354	0.4	0.7	0	11	a1	1357/ 1355	ring stretch
89	1441	0.5	0.9	0.1	19	a1	1419/ 1419	ring stretch
93	1485	0.9	1.5	0.3	55	a1	-/-	ring stretch

94	1500	1.7	3	0.3	223	a1	1501/ 1498	ring stretch
98	1569	0.6	1	0	24	a1	-/-	ring stretch
105	1817	2.4	1.5	0.1	145	b2	1675/-	C=O antisymmetric stretch
106	1821	0.5	0.3	1.0	21	a1	-/1671	C=O symmetric stretch

### **8.13-BENZO[A]NAPHTHACENEDIONE**

The vibrational spectrum of Q5 is discussed here for the first time.

#### **C=O group vibrations**

In Q5 the carbonyl stretching vibrations are still among the strongest in the spectrum. In the infrared spectrum the antisymmetric carbonyl stretch is the second most intense band and is observed at  $1673\text{ cm}^{-1}$ . This band is also observed in the Raman as a weak shoulder at  $1674\text{ cm}^{-1}$ . The symmetric stretch is the only one observed in the Raman spectrum, and is the most intense band in the spectrum, observed at  $1660\text{ cm}^{-1}$ .

#### **C-C ring stretching vibrations**

The most intense vibration seen in the infrared is the ring stretching vibration observed at  $1290\text{ cm}^{-1}$ . This band is also observed in the Raman but only with a very weak intensity. Ring stretching vibrations in the infrared are observed at  $1461\text{ cm}^{-1}$  and  $1456\text{ cm}^{-1}$  albeit with low relative intensities. The band at  $1455\text{ cm}^{-1}$  is also observed as a medium intensity band. At  $1370\text{ cm}^{-1}$  a band is observed in both the Raman and infrared spectra. This band is also assigned as a ring stretching mode with significant CH bending contributions. In the Raman another in plane vibrational mode is observed at  $1155\text{ cm}^{-1}$ . This band is also weakly observed in the infrared spectrum.

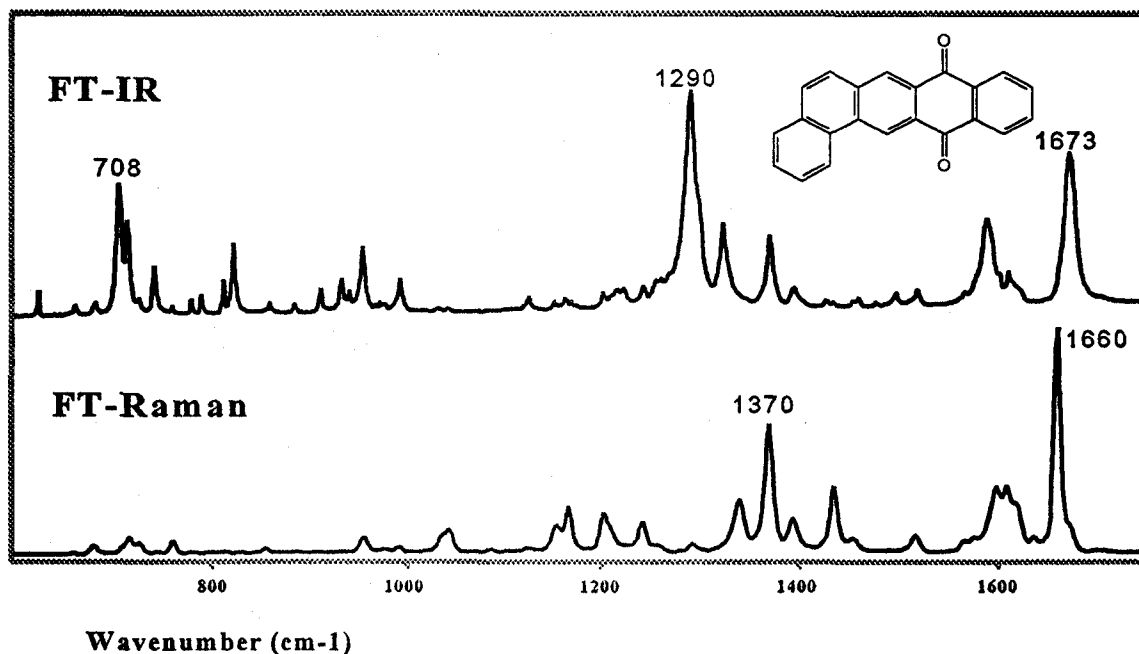
#### **Out of plane vibrations**

With the loss of the C2 symmetry axis going from Q3 to Q5 all of the out of

plane vibrational modes are allowed in the infrared spectrum. Experimentally at least two well defined out-of-plane vibrations are seen. The C-H wagging at 715  $\text{cm}^{-1}$  and 823  $\text{cm}^{-1}$  respectively.

**Figure 3.5**

**8,13-BENZO[A]NAPHTHACENEDIONE (Q5)**



A summary of observed vibrational frequencies for Q5 are given in table 3.5.

**Table 3.5**

**Q5 Observed Vibrational Assignment**

Mode	Fre- quency scaled ( $\text{cm}^{-1}$ )	$\mu_y$ short axis	$\mu_z$ long axis	$\mu_x$ out of plane	Inten- sity (km /mol)	Sym- metry	IR/ Raman ( $\text{cm}^{-1}$ )	Assignment
15	364	0.4	0.7	0	13	$a'$	-/301	skeletal deformation
32	675	0.1	0.1	1.6	51	$a''$	627/-	op C=O bend

34	710	0	0	0.8	11	a''	683/ 683	ring deformation
38	752	0.1	0.1	0.8	12	a''	717/ 718	CH wag
40	792	0	0	1.0	18	a''	743/-	ring deformation
45	861	0	0	0.8	11	a''	823/-	CH wag
53	1005	0.7	1.0	0	28	a'	933/ 933	ring deformation IP
54	1034	0.4	0.8	0	15	a'	955/ 956	ring deformation
62	1129	0.7	0.6	0	16	a'	1110/-	CH bend IP
63	1157	0.2	0.8	0	13	a'	1152/ 1155	ring deformation
69	1248	0.5	1.1	0.2	29	a'	1222/-	ring deformation
72	1315	1.2	2.0	0.2	104	a'	1292/ 1292	ring breathing
75	1406	1.0	1.2	0.1	46	a'	1371/ 1371	ring stretch
78	1469	0.6	0.9	0	21	a'	1456/ 1455	ring stretch
80	1496	1.2	1.9	0.2	91	a'	1461/-	ring stretch
89	1821	2.6	1.6	0.1	169	a'	1671/ 1674	C=O antisym
90	1825	0.9	0.2	0.4	17	a'	-/1660	C=O symmetric stretch



## 7-METHYL-6,15-BENZO[A]NAPHTHACENEDIONE

### C=O group vibrations

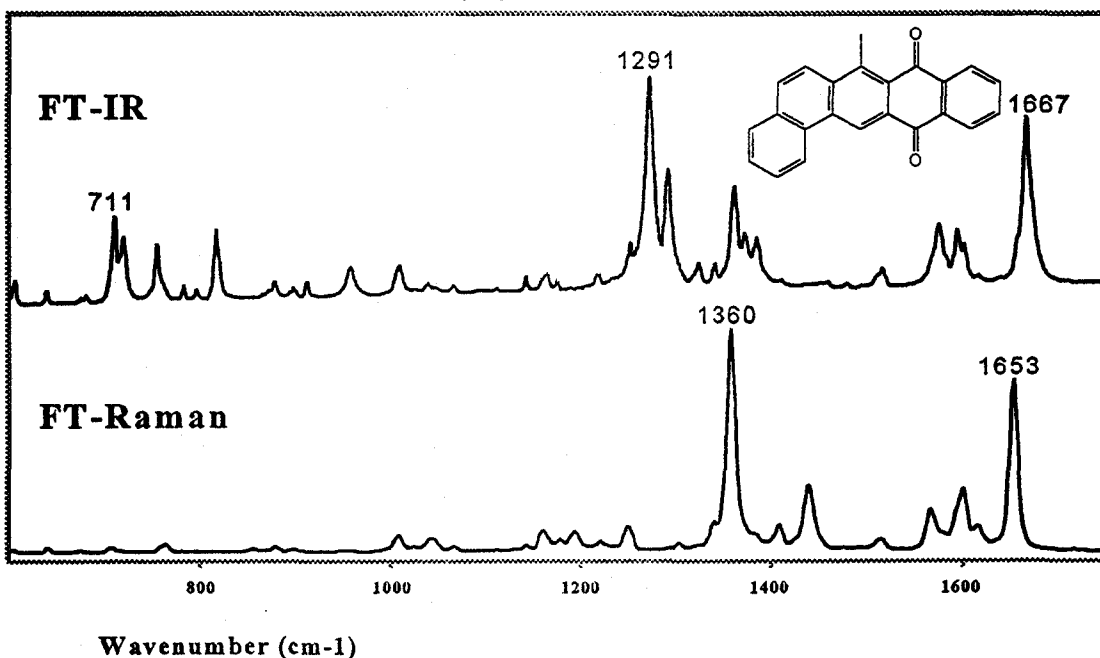
The antisymmetric carbonyl stretching vibration is observed as a very strong band in the infrared at  $1667\text{ cm}^{-1}$ . The symmetric stretching mode of this bond is observed as a strong band in the Raman at  $1653\text{ cm}^{-1}$  and can be observed as a very weak shoulder off of the antisymmetric band in the infrared.

### C-C ring stretching vibrations

The vibration observed at  $1291\text{ cm}^{-1}$  is the most intense vibration in the infrared spectrum, and is attributed to the ring stretching vibration. This band is not observable in the Raman spectrum. The most intense vibration seen in the Raman is observed at  $1360\text{ cm}^{-1}$ . This band is assigned to a ring stretching mode with significant CH bending contributions and is also observed with medium relative intensity in the infrared spectrum. Ring stretching vibrations are also observed in the infrared at  $1325\text{ cm}^{-1}$ , and  $1385\text{ cm}^{-1}$ , with the latter band also observable weakly in the Raman.

**Figure 3.6**

### **7-METHYL-8,13-BENZO[A]NAPHTHACENEDIONE (Q6)**



### Bending vibrations

The addition of a methyl group to Q5, producing Q6, results in the loss of the molecular plane as a symmetry element. All vibrational modes are thus allowed in the infrared and Raman. Experimentally two well defined vibrations are observed at 711 cm<sup>-1</sup> and 820 cm<sup>-1</sup> in the infrared. These are attributed to CH wagging modes and they are weakly observed in the Raman. A summary of observed infrared and Raman vibrations is given in table 3.6

Table 3.6

#### Q6 Observed Vibrational Assignment

Mode	Frequency (scaled) (cm <sup>-1</sup> )	$\mu_y$ short axis	$\mu_z$ long axis	$\mu_x$ out of plane	Intensity (km/mol)	Symmetry	IR/Raman (cm <sup>-1</sup> )	Assignment
19	380	0.3	0.6	0	8	a	-/314	C=O bend
35	678	0.1	0.2	1.4	35	a	553/551	C=O bend
38	718	0	0	1.1	21	a	600/-	molec deform
41	753	0.1	0.1	0.6	6	a	642/642	ring deform
43	793	0	0	1.1	23	a	721/-	CH wag
62	1079	0.4	0.7	0.1	12	a	995/-	CH bend
64	1091	0.5	0.9	0.1	19	a	1008/1006	CH bend
65	1105	0	0.7	0	10	a	1045/1042	ring deform
66	1127	0.3	0.5	0	7	a	1066/1066	CH bend

70	1207	0.5	0.7	0	14	a	1142/ 1143	ring- breath
74	1248	0.5	0.9	0.2	21	a	1175/ 1178	ring deform
77	1310	0.3	0.8	0.1	14	a	1252/ 1249	ring deform
78	1316	0.9	0.7	0.3	67	a	1273/-	ring deform
79	1331	0.9	1.1	0.1	41	a	1291/-	ring breath
82	1404	0.9	1.1	0.1	36	a	1325/-	ring deform
87	1497	1.1	2.1	0.2	107	a	1385/ 1382	ring str
96	1824	2.5	1.3	0.3	156	a	1667/-	C=O antisym
97	1829	0.1	0.7	1.1	32	a	-1653	C=O symm

### Characteristic group frequencies

For analytical applications the concept of characteristic vibrational frequencies is extremely useful. In general, well defined vibrational modes of functional groups maintain an almost invariant wavenumber in a series of molecules. Some modes, have both a characteristic wavenumber and a characteristic relative intensity. Therefore, a grouping of characteristic wavenumbers is one of the benefits of carrying out the vibrational assignment of series of related compounds.

In the series of aromatic quinones studied in this work all of the molecules have a large number of vibrational modes. Nevertheless, it is fairly easy to identify a small group of strong infrared and Raman bands that have characteristic wavenumbers and relative intensities through the whole series. Table 3.7 has

been constructed with a collection of the characteristic vibrational modes in this series of quinones.

**TABLE 3.7**

Characteristic frequencies. (In  $\text{cm}^{-1}$ )

COMPOUND	C=O stretch	Ring Stretch	Out-of-Plane C=O wag + C-H wag
Q1	1659 Raman 1669 IR	1295	702
Q2	1659 Raman 1676 IR	1296	709
Q3	1656 Raman 1675 IR	1292	not observed
Q5	1660 Raman 1673 IR	1290	708
Q6	1653 Raman 1667 IR	1291	711

High frequency vibrations, such as C-H stretching are a generic case of characteristic modes, and are not included here. In the series of aromatic quinones the carbonyl stretching vibrations have characteristic wavenumbers and are also observed with similar relative intensities. The totally symmetric C=O stretch is observed as a strong band in the Raman scattering spectra with a frequency ca.  $1659 \text{ cm}^{-1}$  through the whole series of molecules. The anti-symmetric mode of the C=O stretch is also characteristic through the whole series at ca.  $1669 \text{ cm}^{-1}$ .

**TABLE 3.8**

Calculated vibrational spectrum of Q2 at HF/6-311G\* level of theory

No.	Symm	Calc. (cm <sup>-1</sup> )	Scaled (cm <sup>-1</sup> )	IR Int. (Km/mole)	RS Int. (Å <sup>4</sup> /amu)	Assignment	ρ
1	b1	28	25	3.0534	0	molecular def	0.75
2	a2	65	58	0	2.1033	ring torsion	0.75
3	b1	69	62	2.2682	3.9366	ring deformation	0.75
4	b2	118	106	0.3008	0.7231	ring deformation	0.75
5	a2	132	118	0	2.994	ring twist	0.75
6	b1	165	148	5.4158	2.1809	ring deformation	0.75
7	a2	179	161	0	0.016	ring deformation	0.75
8	b1	213	192	0	2.1159	ring deformation	0.75
9	b2	248	223	0.008	0.214	C-H rock	0.75
10	a1	256	230	0.2283	3.9912	ring stretch	0.18
11	b1	316	284	0.0768	11.735	ring deformation	0.75
12	b2	320	288	1.0166	1.9037	ring deformation	0.75
13	a2	330	297	0	0.1405	ring twist	0.75
14	a1	416	374	39.8047	0.5378	C=O bend	0.4
15	b1	428	385	0.5139	0.2027	ring deformation	0.75

16	b2	442	398	0.3133	0.5405	ring deformation	0.75
17	b2	475	427	0.1472	1.6659	ring deformation	0.75
18	b1	479	431	0.002	1.4678	C-H bend	0.75
19	a1	484	435	7.3976	35.927	ring breath	0.25
20	a2	500	450	0	0.9794	ring twist	0.75
21	b1	528	475	19.4796	0.017	ring bend	0.75
22	b1	537	483	0.3408	6.2866	ring bend	0.75
23	a1	542	487	20.3713	0.7541	ring breath	0.13
24	a2	575	517	0	0.063	ring deformation	0.75
25	b2	598	538	1.8424	4.8808	ring deformation	0.75
26	a2	656	590	0	1.4858	C=O bend	0.75
27	a1	666	599	1.2666	7.3684	ring stretch	0.57
28	a1	690	621	3.2817	0.93	ring stretch	0.23
29	b2	721	648	1.1098	0	ring stretch	0.75
30	a1	735	661	5.114	4.7794	ring stretch	0.38
31	b2	744	669	0.0871	0.4926	ring deformation	0.75
32	a2	769	692	0	0.077	ring torsion	0.75
33	b1	804	723	119.446	0.1003	C=O bend, C-H wag	0.75
34	a2	816	734	0	0.1139	ring torsion	0.75
35	a1	828	745	0.0995	53.435	ring deformation	0.1

36	b2	833	749	2.0608	0.1257	ring deformation	0.75
37	b1	840	756	29.5007	5.9824	C-H bend	0.75
38	a2	849	761	0	10.26	Ring twist	0.75
39	a1	881	792	17.1129	2.8839	C-H bend	0.66
40	b1	895	805	11.3431	0.2612	C-H bend	0.75
41	a2	896	806	0	0.012	C=O bend	0.75
42	a2	949	854	0	2.0529	ring torsion	0.75
43	b2	977	879	0.3903	5.8534	ring deformation	0.75
44	b2	997	897	2.3096	0.021	ring deformation	0.75
45	b1	1000	900	29.8035	2.454	ring torsion	0.75
46	a2	1016	914	0	0.8503	ring torsion	0.75
47	a2	1024	921	0	1.6792	C-H bend	0.75
48	a1	1053	947	217.057	21.072	C=O bend	0.15
49	a2	1074	966	0	0.6598	C-H bend	0.75
50	a1	1076	968	4.1265	5.1054	C-H bend	0.15
51	b1	1079	971	34.3005	10.798	C-H bend	0.75
52	b1	1101	991	7.2224	1.4831	C-H bend	0.75
53	b1	1118	1006	3.0616	0.036	C-H bend	0.75
54	a2	1126	1013	0	2.2928	C-H bend	0.75
55	a1	1142	1028	6.0439	43.115	C-H bend	0.18
56	a2	1144	1029	0	0.2621	C-H bend	0.75
57	a1	1155	1039	0.1274	44.996	C-H bend	0.44
58	b2	1192	1072	0.1542	0.7377	ring deformation	0.75

59	b2	1226	1103	0.01	2.7364	C-H bend	0.75
60	a1	1232	1108	3.3781	15.04	C-H bend	0.58
61	b2	1239	1115	1	0.01	C-H bend	0.75
62	a1	1276	1148	20.8134	195.6	C-H bend	0.29
63	a1	1291	1161	1.13821	23.955	C-H bend	0.2
64	b2	1303	1172	2.3526	16.023	C-H bend	0.75
65	b2	1344	1209	3.3288	24.646	C-H bend	0.75
66	a1	1351	1215	113.469	8.9785	C-H bend	0.16
67	a1	1371	1233	88.1715	358.77	ring breath and C-H bend	0.24
68	b2	1384	1245	2.3375	0.8089	ring deformation	0.75
69	b2	1399	1259	3.987	4.0706	ring deformation	0.75
70	a1	1408	1267	366.708	11.367	ring deformation	0.3
71	b2	1419	1277	0.9691	0.3565	ring deformation	0.75
72	b2	1431	1287	15.5896	23.027	ring deformation	0.75
73	a1	1433	1289	448.838	174.18	ring stretch	0.18
74	b2	1503	1352	0.1394	11.011	ring deformation	0.75
75	a1	1549	1394	5.9318	135.77	C-C stretch	0.22
76	a1	1579	1421	111.123	1367.6	C-C stretch	0.25
77	b2	1600	1440	0.1756	0.04	C-C stretch	0.75
78	a1	1612	1450	124.8	795.13	C-C stretch	0.33



79	b2	1621	1458	0.1001	4.6143	C-C stretch	0.75
80	a1	1634	1470	0	86.946	C-C stretch	0.54
81	a1	1653	1487	5.0912	3.9249	C-C stretch	0.17
82	a1	1727	1554	81.3493	60.788	ring stretch	0.35
83	a1	1763	1586	15.0159	112.4	ring stretch	0.17
84	a1	1775	1597	5.7568	4.6364	ring stretch	0.7
85	b2	1780	1602	6.5119	7.2172	ring stretch	0.75
86	b2	1799	1619	40.935	119.7	ring stretch	0.75
87	b2	1821	1638	2.6381	11.965	ring stretch	0.75
88	b2	1848	1663	6.1229	7.5896	ring stretch	0.75
89	b2	1967	1770	449.609	2.61	C=O stretch	0.75
90	a1	1968	1771	49.3126	526.36	C=O stretch	0.2
91	b2	3357	3189	0.138	14.421	C-H stretch	0.75
92	a1	3361	3192	0.2493	17.801	C-H stretch	0.33
93	b2	3363	3194	10.8195	1.2988	C-H stretch	0.75
94	a1	3367	3198	0.002	180.29	C-H stretch	0.54
95	b2	3368	3199	5.5318	87.43	C-H stretch	0.75
96	b2	3379	3210	38.5341	134.36	C-H stretch	0.75
97	a1	3386	3216	32.8963	260.03	C-H stretch	0.29
98	a1	3391	3221	48.8573	410.28	C-H stretch	0.14
99	b2	3401	3230	0.1651	0.8066	C-H stretch	0.75
100	a1	3402	3231	0.4157	95.455	C-H stretch	0.24
101	b2	3416	3245	1.2751	24.42	C-H stretch	0.75
102	a1	3417	3246	10.8829	176.58	C-H stretch	0.12

## REFERENCES

- 1 N.S.Strokach, T.V. Kainkova, D.N.Shigorin. *Russ. J. Phys. Chem.* **1986**, 70, 63.
- 2 F.A.Cotton. *Chemical Applications of Group Theory 3rd ed.* J.Wiley and Sons, Toronto, (1990).
- 3 A.P. Scott, L. Radom. *J. Phys. Chem.* **1996**, 100, 16502.
- 4 S.N.Singh, R.S.Singh. *Spectrochimica Acta*, **1968**, 24A, 1591.
- 5 Mat Halls, unpublished data, calculated frequencies and geometries of 5,14-pentacenedione.
- 6 *Gaussian 94*, Revision C.3, M.J. Frisch, G.W. Trucks, H.B. Schlegel, P.M.W. Gill, B.G. Johnson, M.A. Robb, J.R. Cheeseman, T. Keith, G. A. Petersson, J.A. Montgomery, K. Raghavachari, M.A. Al-Laham, V.G. Zakrzewski, J.V. Ortiz, J.B. Foresman, J. Cioslowski, B.B. Stefanov, A. Nanayakkara, M. Challacombe, C.Y. Peng, P.Y. Ayala, W. Chen, M.W. Wong, J.L. Andres, E.S. Replogle, R. Gomperts, R.L. Martin, D.J. Fox, J.S. Binkley, D.J. Defrees, J. Baker, J.P. Stewart, M. Head-Gordon, C. Gonzalez, and J.A. Pople, Gaussian, Inc., Pittsburgh PA, 1995.

## **Surface Enhanced Vibrational Spectroscopy**

Surface-enhanced vibrational spectroscopy (SEVS) is the study of molecular vibrations of molecules adsorbed on surfaces that can enhance the absorption and the emission of electromagnetic radiation. The first occurrence of surface enhanced Raman scattering (SERS) was reported by Fleischmann [1] who attributed the intense Raman scattering of pyridine on an electrode to an increase in surface area that is produced in the oxidation/reduction cycle. This explanation was disputed by Creighton [2], and Van Duyne [3] who showed that the growth in surface area due to electrochemical cycling could not account for the great increase in observed intensity. They proposed that the adsorbed pyridine molecules on the electrode surface resulted in an increase in the Raman scattering cross section. In 1982 the first book dedicated to surface enhanced Raman scattering was published [4] containing a variety of models used to explain the origin of the phenomenon. Two factors have been determined to contribute to the observed enhancement in SERS. The main effect is an electromagnetic enhancement that arises from an amplification of the electric field near a roughened metal surface. There is also the possibility of a chemical effect, that only occurs when the molecule of interest is chemically adsorbed onto the metal surface. The three main factors that affect the electromagnetic enhancement are type of metal used, degree of surface roughness, and wavelength of the exciting laser used. For the first factor many different metals have been used, Ag, Au, Pt, Ni, Cu, Pd, to list a few, with Ag and Au being the most common for colloidal, island film, and electrochemical experiments. Surface roughness is a requirement for the observation of SERS. Smooth metal films, or rough films that have undergone annealing do not give rise to any Raman enhancement. The size and shape of particles involved also play an important role in the magnitude of enhancement observed. In colloidal systems the metal particles are approximated as spheres, where in metal island films the particle

shape is approximated by spheroids. These spheroids are further classified as prolate with semi-major axis > semi-minor axis, or oblate with semi-major axis < semi-minor axis. The particles in a system are not completely homogeneous in size or shape, but the average size is smaller or comparable to the wavelength of the exciting laser. Twenty years after its discovery, surface-enhanced Raman scattering (SERS) is a well developed analytical technique. Its development and the initial efforts are compiled in two basic reference books [4,5]. The theory and the experimental properties of SERS have been discussed in several reviews [6-8].

The two complementary components of SEVS are: Surface-enhanced Raman scattering (SERS) and surface-enhanced infrared (SEIR). Recently, it has been experimentally demonstrated that surface enhancement can be observed on isolated nanoparticles as well as on aggregates of nanoparticles[9]. The ultimate goal of single molecule detection seems to be possible thanks to the realization of very large SERS cross sections[9,10]. However, the interpretation of the observed SEV spectra could be challenging. Even the apparent trivial case of identical un-enhanced and enhanced spectra need to be explained. Surface enhancement increases the signal from the analyte. However, drastic alterations of relative intensities may lead to a very different spectrum. For instance, *chemisorption* of the adsorbate leads to a "new" spectrum: the spectrum of the surface complex. Even if the analyte is physisorbed, but assumes a preferred orientation at the surface, then the relative intensities of certain bands may be preferentially enhanced [11-13]. For analytical applications of surface-enhanced vibrational spectroscopy, it seems necessary to develop a standard database of reference spectra for many compounds.

## **A - Surface enhanced Raman spectra of quinones.**

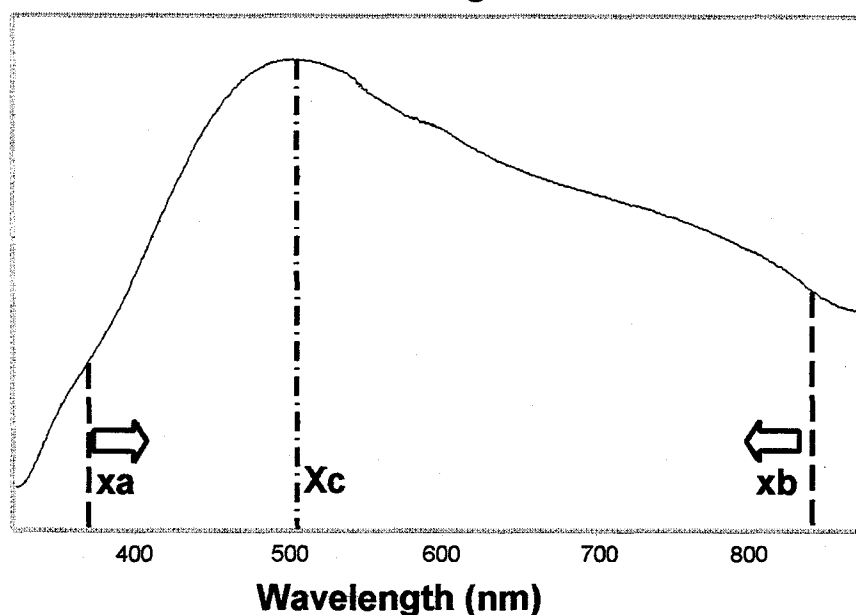
Here we described the SERS of two quinones Q2 and Q6 that represent the best results obtained during the present work on the SERS spectra of quinones on

silver island films.

Metal island films can be tailored to obtain maximum enhancement for a given system. The size and shape of the metal particles in the system greatly affect the surface plasmon modes that are present in the rough metal surfaces. It is a

**Figure 4.1**

**UV-VIS of a 6nm Ag islands film**



coupling of the exciting laser line with these radiative plasmons that gives rise to the electromagnetic effect. The surface plasmon can be experimentally determined using uv-vis spectroscopy. Shown in Figure 4.1 is the plasmon absorption of a 6 nm silver island film prepared by evaporating silver metal at a rate of 0.05 nm/s onto a glass slide maintained at 200°C. A laser frequency in resonance with the absorption of the surface plasmon will give rise to electromagnetic enhancement. It can be seen in the figure that any laser lines within the range from xa to xb nm will give rise to SERS with a maximum occurring at Xc. For reproducibility of results it is important to create equivalent island films. UV-vis spectroscopy provides a

means of monitoring the size and shape of the metal islands and the corresponding surface plasmon absorption of the films.

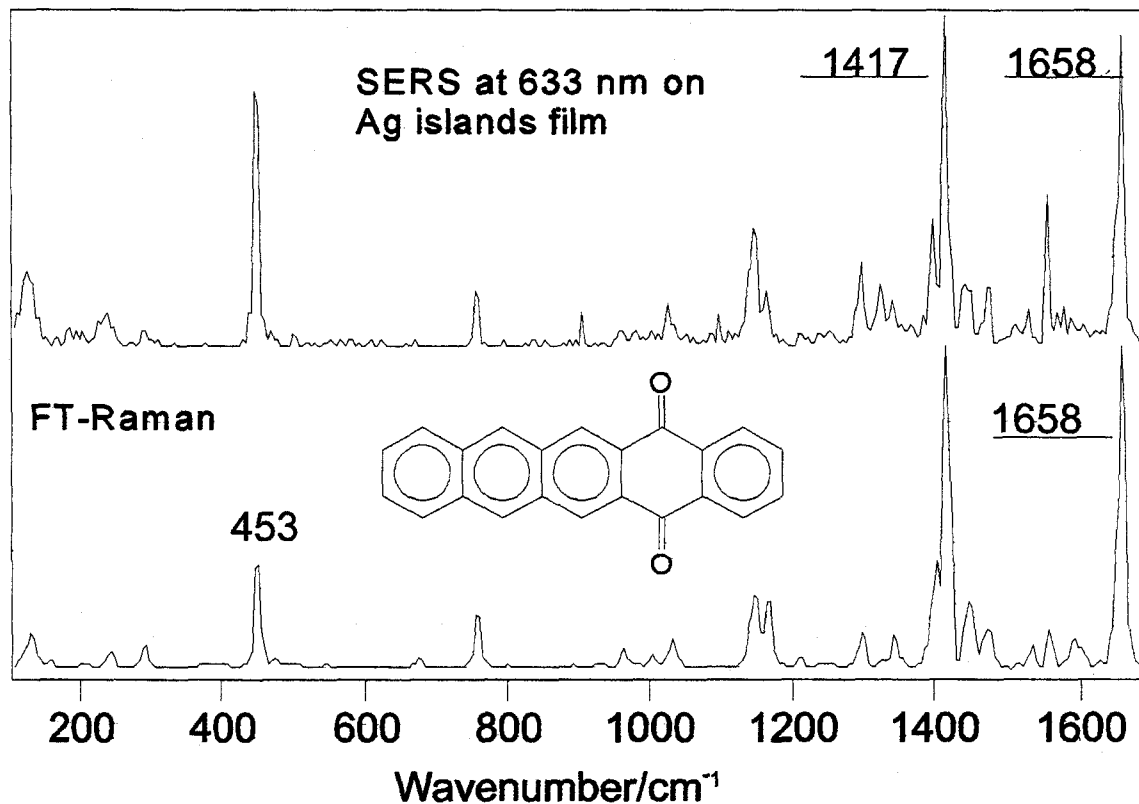
The SERS spectra of Q2 was obtained for a vacuum evaporated film of the organic material onto silver island films and excited with a laser line at 633 nm (Figure 4.2). The surface-enhanced Raman scattering of Q6 was obtained for a single monolayer on silver islands using the 1064.1 nm laser line in an FT-Raman system.

#### Surface-enhanced Raman scattering of Q2.

The SERS of Q2 was obtained from the quinone vacuum evaporated onto a silver island film of 6 nm mass thickness and the FT-Raman spectrum excited with the 1064 nm laser line are presented in Figure 4.2. It can be seen that the observed Raman wavenumbers are exactly the same in both spectra. Two of them are indicated in the figure. The observation of Raman bands that are altered in frequency by the rough metal surface is a clear evidence of a weak interaction of the organic with the metal surface. It can be concluded that the Q2 molecule is physically adsorbed onto the silver islands. There are, however, changes in the observed relative intensities. Since both laser lines are far from resonance with the electronic transitions of Q2, the variations in relative intensities with respect to the bulk can be rationalize in terms of molecular orientation at the metal surface. Molecular vibrations with a polarizability derivative component perpendicular to the metal surface are preferentially enhanced in the near infrared region of the Raman spectrum.

**Figure 4.2**

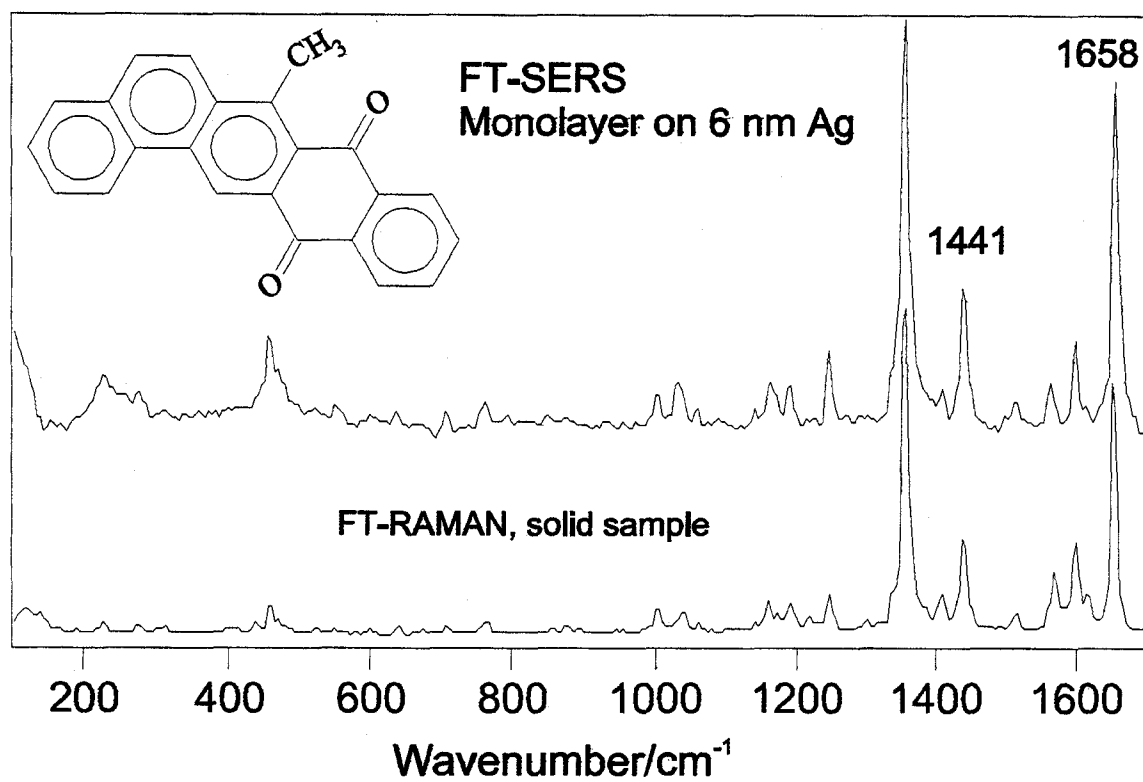
**SERS and FT-Raman of Q2**



The vibrational spectra of Q6 was discussed in Chapter 3. For this material it was possible to fabricate Langmuir monolayers and the floating layers were transferred to glass substrates and glass coated with a 6 nm silver island film. The surface-enhanced Raman obtained for a single monolayer of Q6 is shown in figure 4.3. Assuming an illuminated area of 10 squared microns, the signal given correspond to  $10^{-16}$  mole or about 10 femtograms of material. It was observed that the FT-SERS spectrum is practically identical with the spontaneous Raman spectrum at 1064 nm. It is therefore concluded, that the Q6 like Q2 is also physisorbed onto the rough metal film.

**Figure 4.3**

**FT-Raman and FT-SERS of Q6**





## **B - Surface-enhanced infrared on silver and tin surfaces.**

An early report by Hartstein et al. [15] showed that silver films could also be used to do surface-enhanced infrared (SEIR). However, SEIR did not reach the same level of development of SERS. In fact, the bulk of the SEIR activity is quite recent and the field is just starting to blossom. It is easy to see that due to the vast body of infrared vibrational data that has been systematically collected for gas, liquid, and solids, any improvement in the sensitivity of surface-infrared spectroscopy is bound to have a major impact in the field of vibrational spectroscopy of molecules on surfaces.

### **The enhancement factor.**

The enhancement of vibrational intensities (Raman or infrared) is commonly discussed in terms of two separate contributions: the electromagnetic enhancement mechanism that has been clearly formulated allowing electrodynamic calculations of the surface-enhanced electric intensities [9-11], and the perturbations in the optical parameters of the adsorbate (chemical effect) [12]. Therefore, observed intensities in SEVS are proportional to the product of these two main contributions that may be written as follows :

$$\text{SERS} \propto |A(\omega_L)|^2 |A(\omega_E)|^2 |\partial\alpha/\partial Q|^2$$

$$\text{SEIR} \propto |A(\omega)|^2 |\partial\mu/\partial Q|^2$$

In SERS the  $A(\omega_L)$  and  $A(\omega_E)$  are the enhanced-absorption and the enhanced-emission factors at the frequencies  $\omega_L$  and  $\omega_E$  respectively. Since SEIR can only benefit from the  $|A(\omega)|^2$  factor, the total SEIR enhancement is expected to be orders of magnitude smaller than the enhancement factor observed in SERS. For instance, In the original report of Hartstein et al. [15] the maximum enhancement

factor (EF) measured for SEIR was 20 using ATR and silver islands. Osawa and Ikeda [12], also report an electromagnetic EF of 20-30 for transmission IR spectra on silver islands and an enhancement factor of 20 to 50 for the case of reflection-absorption SEIR [13]. In our own SEIR work on silver island films the optimum EF was found to be ca. 30 [14]. In the present work the best EF factor measured for Sn island films was 20.

### **The substrate.**

According to the electromagnetic mechanism used for the evaluation of the enhancement factor on rough surfaces, the activity of the **substrate** strongly depends on the *shape* of surface protrusions (or metal particles) and the *dielectric function* of the material in the spectral region of interest. In the visible, silver is the most commonly used SERS substrate [16], and silver surfaces continue to be actively investigated by many groups [17]. Single particle models and the effective medium theories can also explain the enhancement observed on silver island films in the infrared [14,18]. It is important to point out that the electromagnetic interpretation also predicts surface enhancement for rough semiconductor surfaces [19], which would allow enhancers for specific regions of the electromagnetic spectrum to be screened. In particular, rough surfaces of tin were never considered as SERS active surfaces in the visible or near-infrared regions of the spectra. In our group Sn was used in SERS experiments to provide the underlying shape in the fabrication of silver coated tin spheres [11]. In this technique, opaque tin films of 150 nm thickness are fabricated to form very regular tin spheres that can be easily coated with silver. Therefore, the tin provides the shape while the silver coating gives the plasmon absorption in resonance with the visible laser excitation, a necessary condition for the local field enhancement.

Tin has a density of 7.2984 grams/cm<sup>3</sup> and the difference between its melting point 231.9 °C and its boiling point 2270 °C, is one of the widest of any metal. The common  $\beta$  phase (white tin) can be easily evaporated to form island

films with regular shape. It is also known that for tin an absorption series exists in the near infrared and in the infrared spectral region. The objective of the present work is to show that tin structures of ultrathin films (18 nm mass thickness) can enhance the absorption of infrared radiation adding a new active **substrate** for SEIR.

### **Surface-enhanced infrared of 5,14-pentacenedione**

The electromagnetic enhancement mechanism (EM) allows one to calculate, to different degrees of approximation, the enhancement that a particular surface could provide for SEVS. It can be found that certain materials can be used to enhance optical properties of adsorbed molecules in the visible, in the near-infrared and/or in the infrared region of the spectrum. Simple calculations show that certain materials, which are not good enhancers in the visible, could be used in the near-infrared region or in the mid-infrared spectral region. Tin, with a low melting point and a high surface tension, can provide island films with very regular particle shape that can be easily fabricated by vacuum evaporation. It is known that tin absorbs light in the near-infrared and infrared regions of the spectrum. These two factors are necessary conditions for enhancement according to the electromagnetic mechanism. Tin island films of varying thicknesses were fabricated and coated with 10 or 15 nm mass thickness of the organic Q2. The enhancement of the infrared absorption spectra was observed for tin films of various thicknesses, however the best results were obtained with tin island films of 15 and 18 nm mass thickness. The SEIR of a 15 nm film of Q2 on 18 nm tin film is shown in Figure 4.4. The spectrum of Q2 film deposited under identical conditions on the substrate without tin is also shown in Figure 4.4 for comparison. The maximum enhancement factor observed was ca. 20. In order to facilitate the discussion of the spectroscopic data, a brief discussion of the vibrational assignment of the observed fundamental vibrational wavenumbers is necessary. The Q2 molecule belongs to the  $C_{2v}$  point group of symmetry with a total irreducible representation

$\Gamma = 35 a_1 + 17 a_2 + 16 b_1 + 34 b_2$ . The infrared active vibrations  $a_1$  are polarized along the  $z$  (long) molecular axis, the  $b_2$  fundamentals are polarized along the  $y$  (short) molecular axis and the  $b_1$  species are the out-of-plane normal modes. The  $a_2$  are not infrared active. Following the report of Brivina et al. [20] for the assignment of normal modes of 5,14-pentacenedione, and with the help of AM1 and PM3 computations of the vibrational spectrum, the assignment of the most intense IR wavenumbers is given in Table 4.1.

**FIGURE 4.4**

SEIR of Q2 on 18nm Sn and 15nm Sn

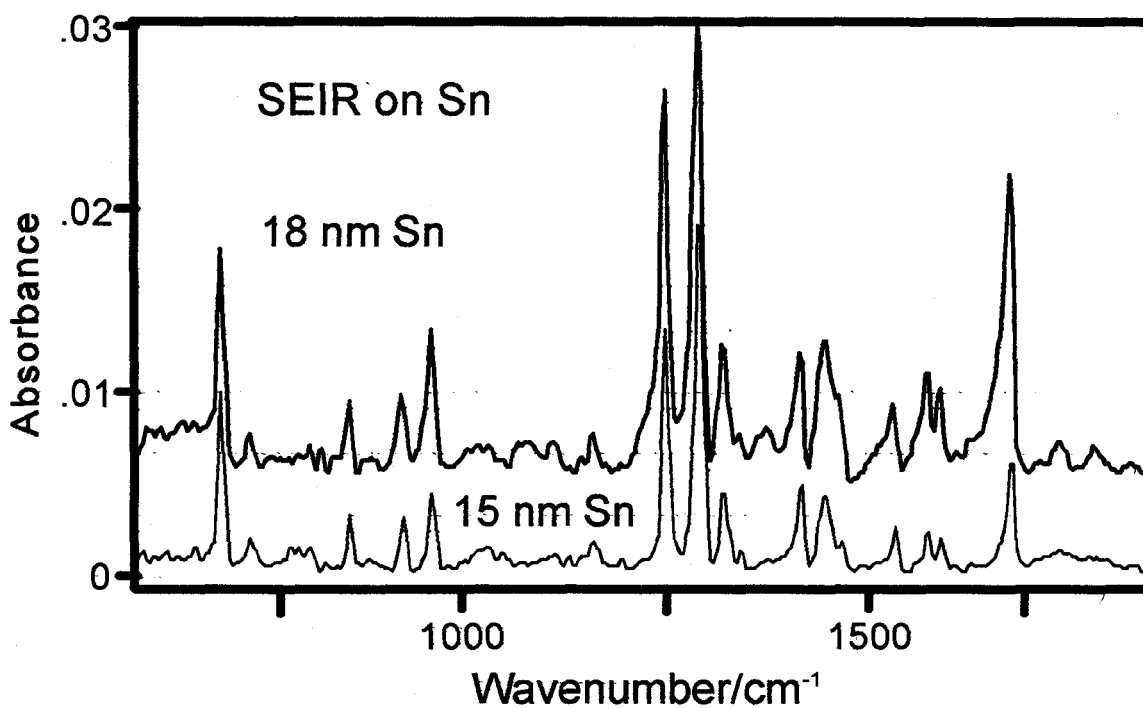


**Table 4.1.**

Internal coordinate assignments for selected infrared wavenumbers of 5,14-pentacenedione (relative intensities in parenthesis).

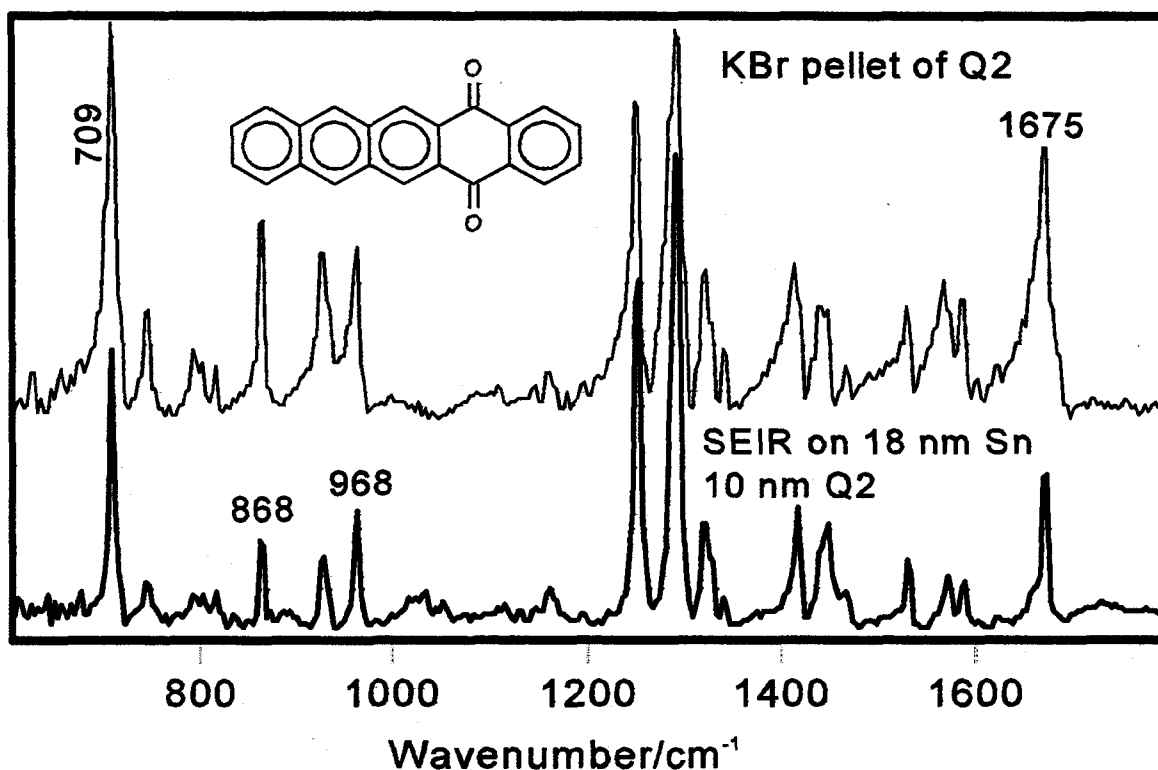
KBr pellet	SEIR	RAIRS	assignment
709 (38)	710 (41)	707 (6)	Out-of- plane wag $b_1$
743 (5)	748 (2)	748 (1)	Out-of- plane wag $b_1$
866 (5)	868 (11)	866 (1)	Out-of-plane wag $b_1$
967 (19)	968 (15)	968 (32)	C-H bending $a_1$
1253 (56)	1254 (52)	1257 (46)	Ring st. + C-H bend $a_1$
1294 (100)	1294 (100)	1299 (100)	Ring st. + C-H bend $b_2$
1323 (19)	1323 (19)	1321 (24)	Ring st. + C-H bend $b_2$
1534 (9)	1533 (10)	1535 (15)	Ring stretch $b_2$
1574 (10)	1576 (5)	1577 (3)	Ring stretch $a_1$
1592 (9)	1593 (4)	1591 (03)	Ring stretch $b_2$
1676 (56)	1676 (18)	1672 (5)	C=O stretch $b_2$

The assignment of in-plane and out-of-plane vibrations is important to describe the properties of the SEIR spectra in comparison with the corresponding reflection-absorption spectra and transmission FTIR spectra of solid matrices and thin solid films. As pointed out in the introduction, the enhancement of the vibrational intensities in the mid-infrared may be the result of two contributions. The enhanced absorption cross section produced by changes in the metal response to electromagnetic radiation, and changes induced in the dipole moment derivatives of each fundamental vibrational mode. The chemical effect or change in the dipole moment derivatives due to the adsorbate-surface interaction can be neglected for physically adsorbed molecules; but it should be carefully examined for chemically adsorbed molecules. Experimentally, chemical adsorption results in frequency shift and/or band broadening, most particularly of the functional group

directly involved in the adsorbate-surface interaction. Figure 4.5, illustrates the comparison between the SEIR spectrum and the spectrum of the Q2 dispersed in a CsI pellet. The observed wavenumbers for the group of intense infrared active vibrations for both spectra is given in Table 4.1. There is no evidence of chemical interaction and the same wavenumbers are measured in the two experimental spectra. It may be concluded that Q2 is physisorbed onto the tin surface and, correspondingly, there is no chemical contribution to the observed enhancement.

The EF found for Q2 on tin is therefore due to the electromagnetic mechanism. The relative intensities of the SEIR spectrum shown in Figure 4.5 are the result of the subtraction of the spectrum of the nanometric film on the IR transparent substrate from the SEIR spectrum of the same film on tin. The analysis of the

**FIGURE 4.5**  
**SEIR and FTIR of Q2**



FTIR transmission spectra given in Figure 4.5 indicates that the SEIR spectrum does not contain any additional bands, or any considerable band shift with respect to those bands present in the IR spectrum of the CsI pellet.

The transmission infrared spectra of nanometric evaporated films of Q2 onto KBr and ZnS substrates show a different pattern of relative intensities when compared with the SEIR as seen in Figure 4.5. The distinct pattern of the spectrum of the film may be due to molecular organization, producing as a result a polarized IR spectrum.

Finally, for a complete characterization of the SEIR on tin two additional experiments were carried out. Firstly, it was important to obtain the RAIRS spectrum on a smooth tin surface. A tin mirror was fabricated by depositing 150 nm of tin onto a glass substrate and then coated with 40 nm of Q2. The RAIRS spectrum is shown in Figure 4.6. The RAIRS of 40 nm Q2 film on a silver mirror is also shown in Figure 4.6. In RAIRS only those vibrational modes with a component of the dipole moment derivative perpendicular to the surface can be observed. Since the out-of-plane vibrational modes observed below  $968\text{ cm}^{-1}$  are present in RAIRS with lower relative intensity, the molecular organization is predominantly with an edge-on or head-on orientation. Identical RAIRS of Q2 on tin and Ag seems to indicate that the same molecular organization exist in the 40 nm organic film formed on smooth tin and Ag. A direct comparison of the SEIR spectrum of Figure 4.4, or the SEIR difference spectrum shown in Figure 4.5, with the RAIRS spectra (Figure 4.6), indicates that the RAIRS surface selection rules can not be directly extended to explain surface-enhanced infrared intensities. Secondly, the SEIR of Q2 on silver island film was also obtained and is presented in Figure 4.7 to be compared with the SEIR on tin. The results are encouraging since the SEIR obtained on two very different substrates are quite similar for the same physisorbed molecule.

**FIGURE 4.6**  
**SEIR and RAIRS of Q2 on Sn**

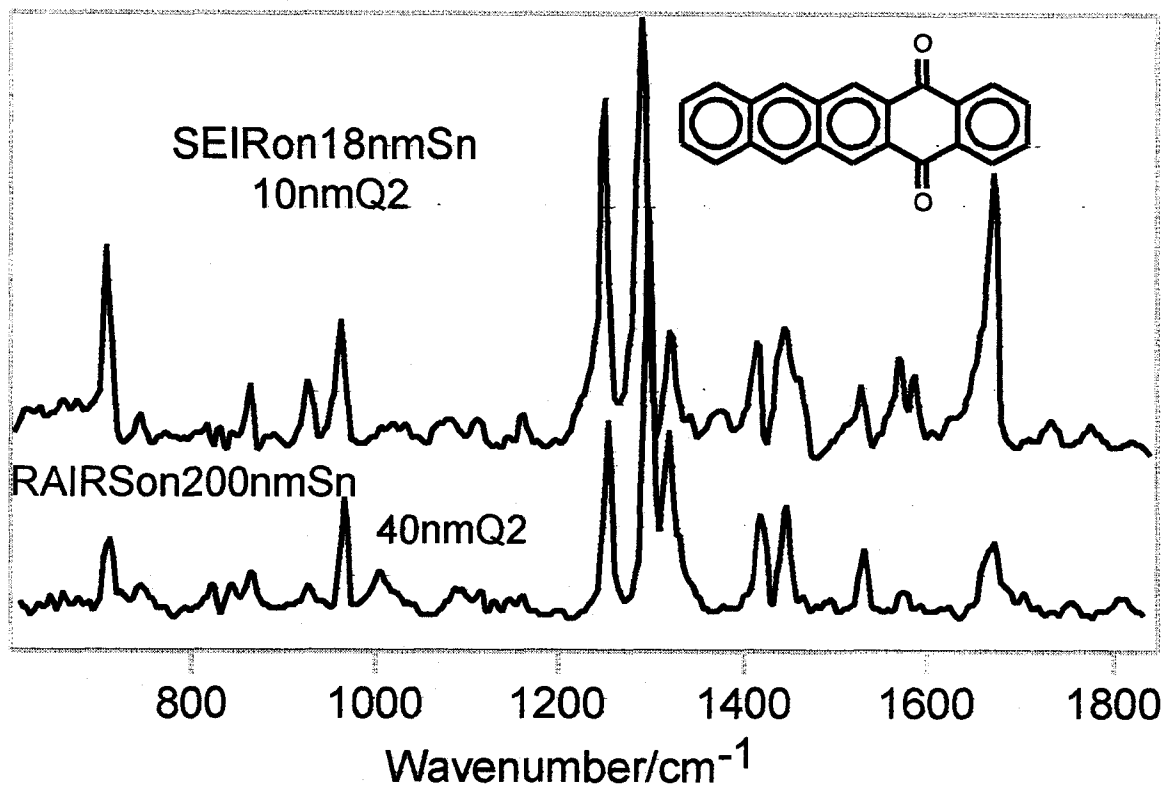
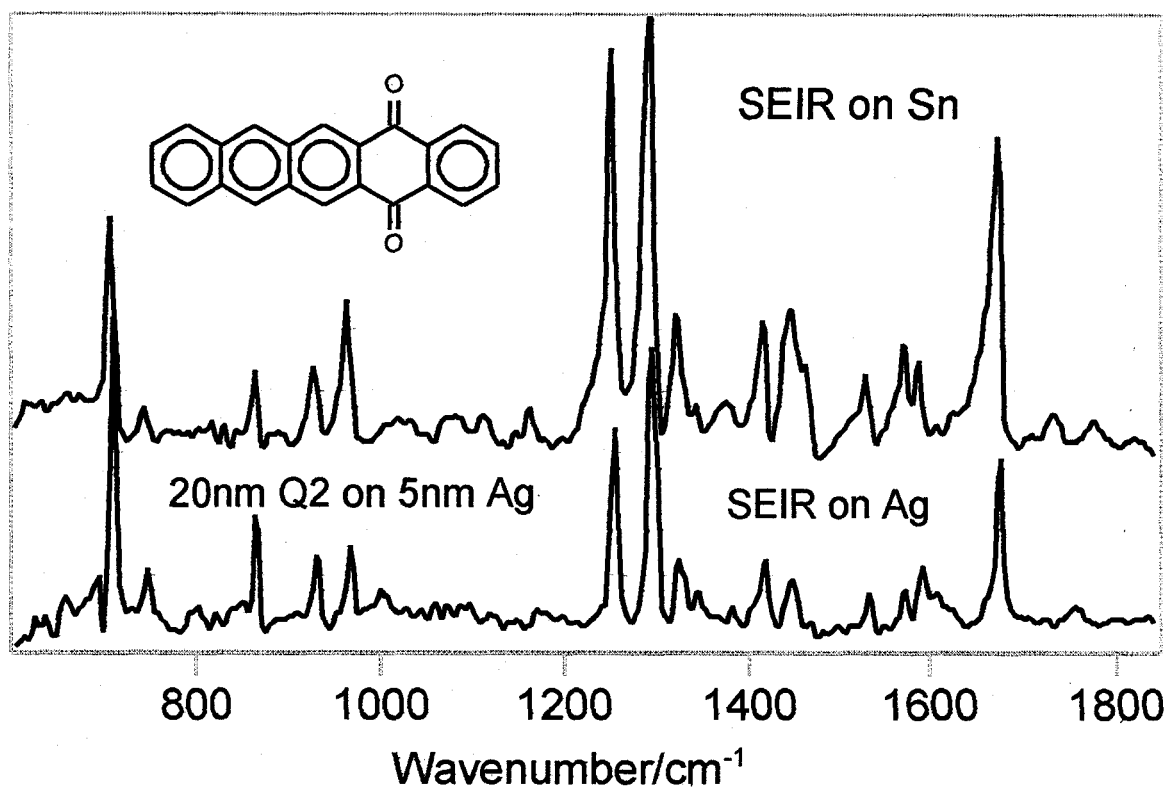




**FIGURE 4.7**  
**SEIR of Q2 on Sn and Ag**



## REFERENCES

1. M. Fleischmann, P.J. Hendra, A.J. McQuillan. *J.Chem.Phys.Lett* **1974**, *26*, 163.
2. M.G. Albrecht, J.A. Creighton. *J. Am. Chem. Soc.* **1977**, *99*, 5215.
3. D.L. Jeanmaire, R.P. Van Duyne. *J.Electroanal.Chem.* **1977**, *84*, 1.
4. *Surface Enhanced Raman Scattering*; R.K. Chang, T.E. Furtak, Eds. Plenum, New York, (1982).
5. *Selected Papers on Surface-enhanced Raman Scattering*, M. Kerker, Editor. SPIE Milestone Series (1990).
6. M. Moskovits. *Rev. Mod. Phys.* **1985**, *57*, 783.
7. R. Aroca, G. Kovacs. in *Vibrational Spectra and Structure*, J.R. Durig, Editor, Elsevier, Amsterdam, (1991), p. 55.
8. A. Otto, I. Mrozek, H. Grabhorn, W. Akeman, *J. Phys. Condens. Matter*, **1992**, *4*, 1143.
9. S. Nie, S.R. Emory, *Science*, **1997**, *275*, 1102.
10. K. Kneipp, Y. Wang, R.R. Dasari, M.S. Feld, *Appl. Spectrosc.*, **1995**, *49*, 780.
11. R. Aroca, S. Rodriguez-Llorente, *J. Mol. Struct.*, **1997**, *408/409*, 17.
12. Osawa, M.; Ikeda, M., *J. Phys. Chem.*, **1991**, *95*, 9914.
13. Nishikawa, Y.; Fujiwara, K.; Ataka, K.; Osawa, M. *Anal. Chem.* 1993, *65*, 556.
14. Johnson, E; Aroca, R., *J. Phys. Chem.*, **1995**, *99*, 9325.
15. Hartstein, A.; Kirtley, J.R.; Tsang, J.C. *Phys. Rev. Lett.*, **1980**, *45*, 201.
16. Efrima, S., *Mod. Aspects Electrochem.*, **1985**, *16*, 253.
17. Semin, D.J.; Lo, A.; Roark, S. E. ; Skodje, R.T.; Rowlen, K.L., *J. Chem. Phys.*, **1996**, *105*, 5542.
18. Osawa, M.; Ataka, K.; Yoshii, K.; Nishikawa, Y. *Appl. Spectrosc.*, **1993**, *47*, 1497.

19. Ueba, H., *Surface Sci.*, **1983**, *133*, L432.
20. Brivina, L.P.; Stokach, N.S., Shirogin, *Russian J. Phys. Chem.*, **1981**, *55(10)*, 1435.

## CONCLUSIONS

The vibrational spectra of 1,4-anthracenedione, 5,14-pentacenedione, 6,15-hexacenedione, 8,13-benzo[a]naphthacenedione, and 7-methyl-8,13-benzo[a]naphthacenedione have been studied using Raman, infrared, and computational methods. The vibrational assignment of fundamental vibrational frequencies are proposed and groups of characteristic frequencies have been identified.

Vacuum evaporated films were fabricated for all the materials under study and Langmuir-Blodgett monolayers of the two largest molecules were also fabricated. A new surface for surface-enhanced infrared studies was developed. It is a rough surface of tin that is fabricated by vacuum evaporation of tin to form island films on infrared transparent substrates. This film has been shown to provide 20x enhancement of intensities in the infrared.

## Appendix A

In the following tables a tentative vibrational assignment for all 5 of the quinones is given. The assignment of the modes was performed by a simulation of the normal coordinate displacement as calculated by hyperchem [1]. For the assignment of the observed vibrational bands the following papers were used as templates for the tentative assignment of these modes [1-7].

## REFERENCES

- 1 B.Lunelli, C.Pecile. *Spectrochimica Acta*, **1973**, 29A, 1989.
- 2 N.S.Strokach, D.N.Shigorin. *Russ. J. Phys. Chem.*, **1977**, 51, 1774.
- 3 N.S.Strokach, T.V. Kainkova, D.N.Shigorin. *Russ J. Phys. Chem.*, **1986**, 60, 63.
- 4 A.Girlando, D.Ragazzon, C.Pecile. *Spectrochimica Acta.*, **1980**, 36A, 1053.
- 5 S.N.Singh, R.S.Singh. *Spectrochimica Acta.*, **1968**, 24A, 1591.
- 6 K.K. Lehmann, J. Smolarok, O.S. Khalil, L. Goodman, *J. Phys. Chem.*, **1979**, 83, 1200.
- 7 L.P. Brivina, N.S.Strokach, D.N.Shigorin. *Russ.J.Phys.Chem.*, **1981**, 55, 1435.

Table A1.1

Q1

Normal Mode #	AM1 corrected	PM3 corrected	FT-IR observed	FT-Raman observed	symmetry	assignment
1	36	57			b <sub>1</sub>	OP C=O bend
2	63	85			a <sub>2</sub>	OP ring torsion
3	86	104			b <sub>1</sub>	OP ring deformation
4	178	189			b <sub>2</sub>	IP C=O bend
5	185	194		186	a <sub>2</sub>	OP ring torsion
6	225	235			b <sub>1</sub>	OP ring deformation
7	250	271			a <sub>2</sub>	OP ring deformation
8	309	306			a <sub>1</sub>	IP ring stretch
9	329	327		317	b <sub>2</sub>	IP ring deformation
10	330	334			b <sub>1</sub>	OP ring deformation
11	415	402			a <sub>1</sub>	IP C=O bend
12	431	425			b <sub>1</sub>	OP ring bend
13	439	443			a <sub>2</sub>	OP ring torsion
14	477	463	445	443	a <sub>1</sub>	IP ring stretch
15	483	479	475	474	b <sub>2</sub>	IP ring bend
16	545	541			a <sub>2</sub>	OP ring deformation
17	564	553	521		b <sub>1</sub>	OP ring deformation
18	567	570	533		b <sub>2</sub>	IP ring deformation
19	595	571	564		a <sub>1</sub>	IP ring stretch
20	630	609			b <sub>2</sub>	IP ring stretch
21	675	675			a <sub>2</sub>	OP ring torsion
22	727	679	669	669	b <sub>1</sub>	OP ring bend
23	731	716			b <sub>2</sub>	IP ring deformation
24	743	726			a <sub>2</sub>	OP ring torsion
25	769	734	702	704	a <sub>1</sub>	IP ring stretch
26	818	797	765		b <sub>1</sub>	OP ring deformation
27	822	805			a <sub>2</sub>	OP ring deformation

Normal Mode #	AM1 corrected	PM3 corrected	FT-IR observed	FT-Raman observed	symmetry	assignment
28	850	807		783	b <sub>2</sub>	IP ring deformation
29	861	851	811	813	b <sub>1</sub>	OP ring deformation
30	878	861			a <sub>2</sub>	OP H bend
31	889	887	845		b <sub>1</sub>	OP H bend
32	892	894	852sh		a <sub>1</sub>	IP ring breathing
33	908	926			a <sub>2</sub>	OP H bend
34	914	934			a <sub>2</sub>	OP H bend
35	1022	976	921		b <sub>2</sub>	IP ring deformation
36	1045	995			a <sub>1</sub>	IP H bend
37	1053	1022	973		a <sub>1</sub>	IP ring deformation
38	1078	1023	1003	1001	b <sub>2</sub>	IP H bend
39	1086	1050	1025	1026	a <sub>1</sub>	IP H bend
40	1113	1072	1052		a <sub>1</sub>	IP H bend
41	1141	1080	1074	1076	b <sub>2</sub>	IP ring deformation + H bend
42	1185	1130			b <sub>2</sub>	IP ring deformation
43	1207	1131		1240	a <sub>1</sub>	IP ring deformation
44	1221	1161	1274	1274	b <sub>2</sub>	IP ring deformation
45	1264	1219	1295	1296	a <sub>1</sub>	IP ring breathing
46	1286	1251			b <sub>2</sub>	IP ring breathing
47	1323	1296	1372		b <sub>2</sub>	IP ring breathing
48	1355	1314		1379	b <sub>2</sub>	IP ring stretch
49	1434	1385	1394	1394	a <sub>1</sub>	IP ring stretch
50	1463	1439	1426	1426	b <sub>2</sub>	IP ring stretch
51	1487	1457		1452	a <sub>1</sub>	IP ring stretch
52	1527	1506			a <sub>1</sub>	IP ring stretch
53	1582	1580	1599		a <sub>1</sub>	IP ring stretch
54	1613	1605	1616	1616	b <sub>2</sub>	IP ring stretch

Normal Mode #	AM1 corrected	PM3 corrected	FT-IR observed	FT-Raman observed	symmetry	assignment
55	1619	1628	1632	1634	b <sub>2</sub>	IP ring stretch
56	1697	1667			a <sub>1</sub>	IP C=C stretch
57	1831	1678	1668		b <sub>2</sub>	IP C=O stretch
58	1834	1697		1658	a <sub>1</sub>	IP C=O stretch
59	2842	2691	3028	3038	b <sub>2</sub>	IP C-H stretch
60	2843	2692			b <sub>2</sub>	IP C-H stretch
61	2845	2693			a <sub>1</sub>	IP C-H stretch
62	2854	2709	3053	3053	a <sub>1</sub>	IP C-H stretch
63	2861	2710			b <sub>2</sub>	IP C-H stretch
64	2864	2714	3066	3068	a <sub>1</sub>	IP C-H stretch
65	2868	2723			b <sub>2</sub>	IP C-H stretch
66	2876	2731		3086	a <sub>1</sub>	IP C-H stretch



Table A1.2

Q2

Mode	AM1 corrected	PM3 corrected	FT-IR	FT-Raman	sym	assignment
1	14.4	19.8			b <sub>1</sub>	OP molecular deformation
2	45.9	42.3			a <sub>2</sub>	OP ring torsion
3	50.4	51.3			b <sub>1</sub>	OP molecular deformation
4	93.6	88.2			a <sub>2</sub>	OP molecular deformation
5	112.5	110.7		94	b <sub>2</sub>	IP molecular deformation
6	129.6	123.3			a <sub>2</sub>	OP ring torsion
7	131.4	124.2			b <sub>1</sub>	OP molecular deformation
8	172.8	162		131	b <sub>1</sub>	OP molecular deformation
9	229.5	224.1			b <sub>2</sub>	IP molecular deformation
10	243	227.7			a <sub>1</sub>	IP molecular deformation
11	243.9	235.8			a <sub>2</sub>	OP ring torsion
12	255.6	247.5		244	b <sub>1</sub>	OP molecular deformation
13	275.4	275.4			b <sub>2</sub>	IP C=O bend
14	315.9	299.7			b <sub>1</sub>	OP molecular deformation
15	365.4	352.8		293	a <sub>1</sub>	IP C=O bend
16	382.5	371.7			b <sub>1</sub>	OP ring deformation
17	390.6	374.4			a <sub>2</sub>	OP ring twist
18	400.5	385.2			b <sub>2</sub>	IP molecular deformation
19	419.4	405			b <sub>1</sub>	OP ring deformation
20	423.9	410.4			b <sub>1</sub>	OP ring deformation
21	438.3	416.7			b <sub>2</sub>	IP ring bend
22	439.2	429.3	452	452	a <sub>1</sub>	IP ring bend
23	440.1	433.8			a <sub>2</sub>	OP ring deformation
24	502.2	478.8			a <sub>2</sub>	OP ring torsion
25	516.6	490.5	462		a <sub>1</sub>	IP ring bend
26	532.8	517.5	504		b <sub>2</sub>	IP ring bend
27	586.8	559.8			a <sub>1</sub>	IP ring deformation
28	606.6	580.5	627		a <sub>1</sub>	IP ring deformation
29	625.5	594.9			a <sub>2</sub>	OP ring torsion
30	636.3	616.5			a <sub>2</sub>	OP ring torsion
31	658.8	646.2			a <sub>2</sub>	OP ring torsion
32	662.4	652.5			a <sub>2</sub>	OP ring torsion

33	674.1	656.1	678	678	b <sub>1</sub>	OP C=O bend
34	678.6	666			a <sub>2</sub>	OP ring torsion
35	720.9	681.3	709		a <sub>1</sub>	IP ring stretch
36	723.6	691.2			b <sub>1</sub>	OP H bend + ring deformation
37	751.5	708.3			a <sub>2</sub>	OP H bend + ring deformation
38	753.3	720	748		b <sub>2</sub>	IP ring deformation
39	774	747.9			a <sub>2</sub>	OP C=O bend
40	814.5	777.6			a <sub>2</sub>	OP molecular deformation
41	825.3	802.8	759	760	b <sub>1</sub>	OP H bend
42	842.4	806.4	795		a <sub>1</sub>	IP ring breathing
43	844.2	811.8			a <sub>2</sub>	OP molecular deformation
44	851.4	814.5	807		b <sub>2</sub>	IP molecular deformation
45	855.9	827.1			a <sub>2</sub>	OP molecular deformation
46	859.5	846.9	821		b <sub>2</sub>	IP molecular deformation
47	871.2	861.3			b <sub>1</sub>	OP H bend
48	885.6	876.6			a <sub>2</sub>	OP H bend
49	886.5	880.2	866		b <sub>1</sub>	OP molecular deformation
50	891.9	882			b <sub>1</sub>	OP H bend
51	905.4	891			a <sub>2</sub>	OP H bend
52	912.6	910.8			a <sub>2</sub>	OP H bend
53	921.6	918.9	933	933	a <sub>1</sub>	IP molecular deformation
54	1024.2	973.8			a <sub>1</sub>	IP molecular deformation
55	1051.2	985.5	968	966	a <sub>1</sub>	IP molecular deformation
56	1064.7	1004.4			b <sub>2</sub>	IP H bend
57	1065.6	1008	1004	1003	a <sub>1</sub>	IP H bend
58	1077.3	1014.3			b <sub>2</sub>	IP H bend
59	1081.8	1029.6			a <sub>1</sub>	IP H bend
60	1089	1038.6	1031	1030	a <sub>1</sub>	IP H bend
61	1110.6	1044			b <sub>2</sub>	IP ring deformation
62	1118.7	1044.9			a <sub>1</sub>	IP ring deformation
63	1149.3	1072.8	1149	1148	b <sub>2</sub>	IP ring deformation
64	1168.2	1091.7	1163		a <sub>1</sub>	IP ring stretch
65	1169.1	1102.5	1166	1166	b <sub>2</sub>	IP ring deformation
66	1179	1115.1			b <sub>2</sub>	IP ring deformation
67	1194.3	1125.9	1181		b <sub>2</sub>	IP ring deformation
68	1209.6	1174.5	1198		a <sub>1</sub>	IP ring deformation

69	1249.2	1195.2	1212	1209	a <sub>1</sub>	IP ring deformation
70	1272.6	1215.9			b <sub>2</sub>	IP ring deformation
71	1296	1250.1	1252	1250	b <sub>2</sub>	IP ring deformation
72	1310.4	1257.3	1293	1296	a <sub>1</sub>	IP ring breathing
73	1329.3	1276.2	1325	1324	b <sub>2</sub>	IP ring deformation
74	1345.5	1288.8	1344	1341	a <sub>1</sub>	IP ring deformation
75	1429.2	1378.8		1400	b <sub>2</sub>	IP ring deformation
76	1432.8	1405.8	1419	1417	a <sub>1</sub>	IP ring deformation
77	1462.5	1442.7	1444	1447	a <sub>1</sub>	IP ring deformation
78	1483.2	1458	1451		b <sub>2</sub>	IP ring deformation
79	1488.6	1461.6	1470	1470	a <sub>1</sub>	IP ring stretch
80	1502.1	1474.2			a <sub>1</sub>	IP ring stretch
81	1517.4	1499.4			a <sub>1</sub>	IP ring stretch
82	1566.9	1562.4	1533	1533	a <sub>1</sub>	IP ring stretch
83	1570.5	1505.7		1558	a <sub>1</sub>	IP ring stretch
84	1592.1	1610.1	1573		b <sub>2</sub>	IP ring stretch
85	1602	1611.9	1592	1590	a <sub>1</sub>	IP ring stretch
86	1615.5	1614.6	1607		b <sub>2</sub>	IP ring stretch
87	1621.8	1645.2			b <sub>2</sub>	IP ring stretch
88	1634.4	1647.9	1626	1626	b <sub>2</sub>	IP ring stretch
89	1818	1754.1	1677		b <sub>2</sub>	IP C=O stretch antisym
90	1821.6	1759.5		1658	a <sub>1</sub>	IP C=O stretch symm
91	2842.2	2729.7	3026		b <sub>2</sub>	IP C-H stretch
92	2844	2730.6		3030	a <sub>1</sub>	IP C-H stretch
93	2850.3	2738.7			b <sub>2</sub>	IP C-H stretch
94	2852.1	2739.6	3050	3050	a <sub>1</sub>	IP C-H stretch
95	2859.3	2740.5			b <sub>2</sub>	IP C-H stretch
96	2861.1	2741.4			b <sub>2</sub>	IP C-H stretch
97	2862	2745	3063	3063	a <sub>1</sub>	IP C-H stretch
98	2862.9	2746.8			a <sub>1</sub>	IP C-H stretch
99	2864.7	2753.1			b <sub>2</sub>	IP C-H stretch
100	2869.2	2758.5			b <sub>2</sub>	IP C-H stretch
101	2873.7	2766.6		3077	a <sub>1</sub>	IP C-H stretch
102	2877.3	2768.4			a <sub>1</sub>	IP C-H stretch

Table A1.3

Q3

Mode	AM1 corrected	PM3 corrected	FT-IR	FT-Raman	sym	assignment
1	11.7	12.6			b <sub>1</sub>	OP molecular deformation
2	43.2	39.6			a <sub>2</sub>	OP molecular deformation
3	51.3	49.5			b <sub>1</sub>	OP molecular deformation
4	63	55.8			a <sub>2</sub>	OP molecular deformation
5	83.7	81			b <sub>1</sub>	OP molecular deformation
6	91.8	91.8			b <sub>2</sub>	IP molecular deformation
7	129.6	122.4			a <sub>2</sub>	OP molecular torsion
8	135.9	130.5		108	b <sub>1</sub>	OP molecular deformation
9	172.8	170.1			b <sub>2</sub>	IP molecular deformation
10	191.7	181.8			a <sub>2</sub>	OP ring torsion
11	198	182.7		189	b <sub>1</sub>	OP molecular deformation
12	231.3	225.9		214	b <sub>1</sub>	OP molecular deformation
13	245.7	236.7			a <sub>2</sub>	OP ring torsion
14	253.8	251.1		244	b <sub>2</sub>	IP C=O bend
15	261.9	254.7			b <sub>1</sub>	OP molecular bend
16	311.4	297.9			b <sub>1</sub>	OP molecular bend
17	326.7	318.6		266	a <sub>1</sub>	IP molecular deformation
18	330.3	321.3			b <sub>2</sub>	IP molecular deformation
19	361.8	349.2		306	b <sub>1</sub>	OP molecular deformation
20	403.2	394.2		326	b <sub>2</sub>	IP molecular deformation
21	419.4	404.1			b <sub>1</sub>	OP molecular deformation
22	423	409.5			a <sub>2</sub>	OP molecular deformation
23	423.9	410.4			b <sub>1</sub>	OP molecular deformation
24	430.2	414			b <sub>1</sub>	OP ring deformation
25	441	425.7			a <sub>2</sub>	OP ring torsion
26	441.9	433.8		366	a <sub>1</sub>	IP molecular deformation
27	462.6	443.7			b <sub>2</sub>	IP molecular deformation
28	476.1	459			a <sub>2</sub>	OP C=O bend
29	478.8	465.3		453	a <sub>1</sub>	IP molecular deformation
30	542.7	522			b <sub>2</sub>	IP molecular deformation
31	561.6	534.6			a <sub>1</sub>	IP molecular deformation
32	569.7	537.3	580	578	b <sub>2</sub>	IP molecular deformation

33	595.8	569.7	606		a <sub>1</sub>	IP molecular deformation
34	608.4	581.4	617		a <sub>1</sub>	IP molecular deformation
35	623.7	612			a <sub>2</sub>	OP ring torsion
36	659.7	637.2			a <sub>2</sub>	OP ring torsion
37	666	648			a <sub>2</sub>	OP ring torsion
38	676.8	657			a <sub>2</sub>	OP ring torsion
39	678.6	662.4			a <sub>2</sub>	OP ring torsion
40	684	665.1	724		b <sub>1</sub>	OP C=O bend
41	690.3	666			b <sub>2</sub>	IP ring deformation
42	723.6	685.8	736	734	b <sub>1</sub>	OP ring deformation
43	728.1	691.2			b <sub>1</sub>	OP ring deformation
44	731.7	700.2	754		b <sub>1</sub>	OP ring deformation
45	774.9	747		758	a <sub>2</sub>	OP C=O bend
46	795.6	756			b <sub>2</sub>	IP ring deformation
47	814.5	777.6			a <sub>2</sub>	OP H bend
48	822.6	792			a <sub>2</sub>	OP H bend
49	824.4	802.8	778	779	b <sub>1</sub>	OP H bend
50	840.6	809.1			a <sub>1</sub>	OP ring deformation
51	852.3	812.7			b <sub>2</sub>	OP ring deformation
52	853.2	820.8			a <sub>2</sub>	OP H bend
53	855.9	836.1	828		b <sub>1</sub>	OP H bend
54	864.9	843.3	834		b <sub>2</sub>	OP ring deformation
55	872.1	844.2			b <sub>1</sub>	OP H bend
56	874.8	863.1	868		a <sub>1</sub>	IP molecular deformation
57	878.4	876.6			a <sub>2</sub>	OP molecular deformation
58	886.23	880.2			b <sub>1</sub>	OP molecular deformation
59	886.41	882	897		b <sub>1</sub>	OP H bend
60	889.2	890.1	912	912	b <sub>1</sub>	OP H bend
61	905.4	892.8			a <sub>2</sub>	OP H bend
62	907.2	913.5			a <sub>2</sub>	OP H bend
63	928.8	916.2	951		a <sub>1</sub>	IP molecular deformation
64	1031.4	984.6	991		a <sub>1</sub>	IP molecular deformation
65	1051.2	988.2		1006	a <sub>1</sub>	IP ring breath
66	1053	990.9	1019	1021	a <sub>1</sub>	IP ring breath
67	1074.6	1010			b <sub>2</sub>	IP H bend
68	1078.2	1014		1147	b <sub>2</sub>	IP H bend

69	1087.2	1030			a <sub>1</sub>	IP H bend
70	1089	1031		1163	a <sub>1</sub>	IP H bend
71	1098	1040	1167		b <sub>2</sub>	IP ring deformation
72	1115.1	1044			a <sub>1</sub>	IP H bend
73	1125.9	1050	1203	1202	b <sub>2</sub>	IP H bend
74	1140.3	1076			a <sub>1</sub>	IP H bend
75	1158.3	1082			b <sub>2</sub>	IP H bend
76	1178.1	1103			b <sub>2</sub>	IP H bend
77	1179	1119		1253	a <sub>1</sub>	IP H bend
78	1186.2	1127			b <sub>2</sub>	IP H bend
79	1193.4	1128	1256		b <sub>2</sub>	IP H bend
80	1213.2	1169			a <sub>1</sub>	IP H bend
81	1247.4	1195	1292		a <sub>1</sub>	IP H bend
82	1268.1	1217			b <sub>2</sub>	IP molecular deformation
83	1289.7	1257	1310		b <sub>2</sub>	IP molecular deformation
84	1305.9	1265			b <sub>2</sub>	IP molecular deformation
85	1338.3	1282			b <sub>2</sub>	IP molecular deformation
86	1339.2	1284	1343	1342	a <sub>1</sub>	IP H bend
87	1354.5	1319	1357	1355	a <sub>1</sub>	IP molecular deformation
88	1425.6	1377	1393	1396	a <sub>1</sub>	IP molecular deformation
89	1440.9	1401	1419	1419	a <sub>1</sub>	IP molecular deformation
90	1462.5	1442	1447	1450	a <sub>1</sub>	IP ring stretch
91	1465.2	1444			b <sub>2</sub>	IP ring stretch
92	1483.2	1457	1473	1471	b <sub>2</sub>	IP ring stretch
93	1485	1462			a <sub>1</sub>	IP ring stretch
94	1500.3	1476	1501	1498	a <sub>1</sub>	IP ring stretch
95	1516.5	1499		1512	a <sub>1</sub>	IP ring stretch
96	1530.9	1512	1533	1533	a <sub>1</sub>	IP ring stretch
97	1566.9	1562	1557	1556	a <sub>1</sub>	IP ring stretch
98	1569.6	1587			a <sub>1</sub>	IP ring stretch
99	1584.9	1601	1573	1574	a <sub>1</sub>	IP ring stretch
100	1610.1	1614	1587	1585	b <sub>2</sub>	IP ring stretch
101	1616.4	1619	1608		b <sub>2</sub>	IP ring stretch
102	1620	1642			b <sub>2</sub>	IP ring stretch
103	1624.5	1645	1623	1622	b <sub>2</sub>	IP ring stretch
104	1635.3	1648			b <sub>2</sub>	IP ring stretch
105	1818	1751	1675		b <sub>2</sub>	IP C=O stretch

106	1820.7	1753		1671	a <sub>1</sub>	IP C=O stretch
107	2843.1	2730			b <sub>2</sub>	IP C-H stretch
108	2844	2731	3025	3025	b <sub>2</sub>	IP C-H stretch
109	2844.9	2732			a <sub>1</sub>	IP C-H stretch
110	2845.8	2732			a <sub>1</sub>	IP C-H stretch
111	2860.2	2741			b <sub>2</sub>	IP C-H stretch
112	2860.83	2741			b <sub>2</sub>	IP C-H stretch
113	2861.1	2745			b <sub>2</sub>	IP C-H stretch
114	2862	2745			a <sub>1</sub>	IP C-H stretch
115	2862.9	2747			a <sub>1</sub>	IP C-H stretch
116	2863.8	2747			a <sub>1</sub>	IP C-H stretch
117	2868.57	2757	3049	3049	b <sub>2</sub>	IP C-H stretch
118	2868.75	2759			b <sub>2</sub>	IP C-H stretch
119	2876.4	2768	3063		a <sub>1</sub>	IP C-H stretch
120	2876.67	2768			a <sub>1</sub>	IP C-H stretch

Table A1.4

Q5

Mode	AM1 corrected	PM3 corrected	FT-IR	FT-Raman	sym	assignment
1	16.2	18.9			a''	OP ring deformation
2	35.1	36			a''	OP ring deformation
3	57.6	61.2		68	a''	OP ring deformation
4	94.5	86.4		78	a''	OP ring deformation
5	112.5	112.5		103	a'	IP ring deformation
6	120.6	123.3		115	a''	OP ring deformation
7	127.8	125.1		127	a''	OP ring deformation
8	171	162.9		149	a''	OP ring bend
9	213.3	212.4		164	a''	OP ring bend
10	220.5	218.7		207	a'	IP molecular deformation
11	261.9	247.5		222	a''	OP molecular deformation
12	267.3	264.6			a''	OP molecular deformation
13	287.1	285.3		270	a'	IP ring deformation
14	331.2	324.9			a''	OP ring deformation
15	364.5	350.1		301	a'	IP C=O bend
16	365.4	355.5			a''	OP molecular deformation
17	389.7	376.2			a''	OP ring bend
18	392.4	383.4			a''	OP ring torsion
19	410.4	391.5		397	a'	IP ring deformation
20	443.7	432			a''	OP ring deformation
21	445.5	436.5		413	a'	IP molecular deformation
22	456.3	440.1		444	a'	IP molecular deformation
23	495	468.9			a''	OP ring deformation
24	496.8	483.3			a''	OP ring deformation
25	504.9	486		459	a''	OP C=O bend
26	511.2	500.4	494	493	a'	IP ring deformation
27	574.2	549.9	515	517	a'	IP ring deformation
28	602.1	576.9	542		a'	IP ring bend
29	608.4	599.4	589		a''	OP ring deformation
30	630.9	602.1			a'	IP ring deformation
31	648	641.7	627		a''	OP ring deformation



32	675	653.4			a''	OP C=O bend
33	693.9	666	665	663	a'	IP C=O bend
34	711	686.7	683	683	a''	OP ring deformation
35	724.5	695.7	685		a'	IP ring deformation
36	733.5	696.6			a''	OP ring deformation
37	735.3	717.3	710		a'	IP molecular deformation
38	752.4	721.8	717	718	a''	OP H bend
39	774	746.1	727	727	a''	OP C=O bend
40	792	761.4	743		a''	OP ring deformation
41	801.9	764.1	761	761	a'	IP molecular deformation
42	828.9	796.5	780	781	a''	OP ring deformation
43	838.8	809.1	790		a'	IP ring deformation
44	846	819	813	814	a''	OP ring deformation
45	861.3	829.8	823		a''	OP H bend
46	864	857.7		856	a'	IP C=O bend
47	871.2	866.7	860		a''	OP H bend
48	878.4	877.5			a''	OP ring deformation
49	891.9	887.4	886	887	a''	OP H bend
50	896.4	899.1			a''	OP H bend
51	905.4	917.1			a''	OP H bend
52	912.6	919.8	912	912	a''	OP H bend
53	1005.3	955.8	933	933	a'	IP molecular deformation
54	1034.1	984.6	955	956	a'	IP molecular deformation
55	1063.8	1000.8	968		a'	IP molecular deformation
56	1065.6	1005.3	971		a'	IP molecular deformation
57	1068.3	1010.7	976	976	a'	IP molecular deformation
58	1075.5	1017			a'	IP H bend
59	1081.8	1033.2	992	991	a'	IP H bend
60	1088.1	1044.9	1031		a'	IP H bend
61	1098.9	1048.5	1041	1044	a'	IP H bend
62	1129.5	1064.7	1110		a'	IP H bend
63	1157.4	1083.6	1152	1155	a'	IP ring deformation
64	1170	1095.3	1163	1166	a'	IP H bend
65	1175.4	1106.1	1170		a'	IP H bend
66	1198.8	1132.2	1202	1203	a'	IP ring deformation
67	1231.2	1170.9			a'	IP H bend
68	1232.1	1193.4	1215		a'	IP ring deformation

69	1248.3	1198.8	1222		a'	IP ring deformation
70	1260.9	1221.3	1243	1242	a'	IP ring deformation
71	1294.2	1224.9	1255	1257	a'	IP ring deformation
72	1314.9	1258.2	1268		a'	IP ring breathing
73	1332	1291.5	1292	1292	a'	IP ring deformation
74	1350	1313.1		1341	a'	IP ring deformation
75	1405.8	1374.3	1371	1371	a'	IP ring deformation
76	1424.7	1400.4	1394	1394	a'	IP ring deformation
77	1435.5	1410.3	1435	1436	a'	IP ring deformation
78	1469.7	1433.7	1456	1455	a'	IP ring stretch
79	1490.4	1460.7	1461		a'	IP ring stretch
80	1495.8	1476			a'	IP ring stretch
81	1515.6	1495.8	1498		a'	IP ring stretch
82	1555.2	1548	1519	1519	a'	IP ring stretch
83	1579.5	1601.1	1568	1567	a'	IP ring stretch
84	1592.1	1610.1	1587		a'	IP ring stretch
85	1601.1	1611			a'	IP ring stretch
86	1609.2	1618.2	1600	1599	a'	IP ring stretch
87	1613.7	1629.9	1609	1608	a'	IP ring stretch
88	1624.5	1638	1621	1618	a'	IP C=C stretch
89	1820.7	1755	1671	1674(sh)	a'	IP C=O stretch antisym
90	1825.2	1760.4		1660	a'	IP C=O stretch symm
91	2844	2688.3	2990		a'	IP C-H stretch
92	2846.7	2711.7		2996	a'	IP C-H stretch
93	2850.3	2730.6	3016	3014	a'	IP C-H stretch
94	2852.1	2738.7			a'	IP C-H stretch
95	2857.5	2739.6	3032	3033	a'	IP C-H stretch
96	2862	2740.5			a'	IP C-H stretch
97	2864.7	2745.9	3045		a'	IP C-H stretch
98	2865.6	2753.1			a'	IP C-H stretch
99	2867.4	2754.9			a'	IP C-H stretch
100	2870.1	2755.8	3063	3064	a'	IP C-H stretch
101	2874.6	2765.7	3071	3072	a'	IP C-H stretch
102	2878.2	2767.5	3088		a'	IP C-H stretch

Table A1.5

Q6

Mode	AMI corrected	PM3 corrected	FT-IR	FT-Raman	sym	assignment
1	20.7	25.2			A	molecular bend
2	27.9	36			A	molecular bend
3	53.1	62.1			A	molecular bend
4	73.8	78.3			A	molecular bend
5	91.8	91.8		84	A	ring torsion
6	104.4	117.9			A	molecular deformation
7	113.4	129.6		119	A	C=O bend
8	137.7	147.6			A	molecular deformation
9	153.9	164.7		140	A	molecular bend
10	189	184.5			A	molecular bend
11	225.9	220.5			A	molecular deformation
12	235.8	235.8		229	A	molecular deformation
13	257.4	243.9			A	molecular deformation
14	271.8	265.5			A	C=O bend + molecular deformation
15	292.5	286.2		279	A	C=O bend + molecular deformation
16	346.5	333.9			A	ring deformation
17	360	342.9		302	A	C=O bend
18	370.8	348.3			A	molecular deformation
19	380.7	364.5		314	A	C=O bend
20	387	368.1			A	ring torsion
21	406.8	396			A	molecular deformation
22	433.8	425.7			A	ring torsion
23	454.5	439.2			A	molecular deformation
24	459.9	450			A	molecular deformation
25	478.8	459.9			A	molecular deformation
26	487.8	470.7			A	molecular deformation
27	495	484.2		441	A	molecular deformation
28	520.2	508.5			A	ring bend
29	533.7	522	462	463	A	molecular deformation
30	558	537.3			A	ring bend
31	589.5	567	491		A	molecular deformation

32	612	603			A	molecular deformation
33	627.3	604.8	522	524	A	molecular deformation
34	655.2	630.9			A	molecular deformation
35	677.7	657	553	551	A	C=O bend
36	685.8	665.1	564		A	molecular deformation
37	699.3	681.3		582	A	molecular deformation
38	718.2	698.4	600		A	molecular deformation
39	732.6	701.1	606	605	A	C-H bend
40	739.8	717.3			A	molecular deformation
41	754.2	728.1	642	642	A	ring deformation
42	781.2	759.6	713		A	ring deformation
43	793.8	761.4	721		A	C-H bend
44	802.8	768.6	756		A	ring breathing
45	828	794.7	763	765	A	ring deformation
46	836.1	809.1	784		A	molecular deformation
47	844.2	817.2	797		A	molecular deformation
48	861.3	830.7	817	817	A	molecular deformation
49	863.1	863.1			A	ring deformation
50	873.9	873.9			A	ring deformation
51	889.2	880.2			A	ring deformation
52	890.1	891			A	ring deformation
53	904.5	904.5	878	879	A	ring torsion + ring deformation
54	911.7	910.8	899	898	A	ring torsion + ring deformation
55	954	917.1			A	ring deformation
56	963	918.9	912		A	ring deformation
57	969.3	934.2			A	methyl bend
58	1054.8	990.9	958	959	A	C-H bend
59	1059.3	999.9	970		A	C-H bend
60	1064.7	1000.8			A	C-H bend
61	1068.3	1008.9			A	C-H bend
62	1080	1025.1	995		A	C-H bend
63	1084.5	1032.3			A	C-H bend
64	1090.8	1039.5	1008	1006	A	C-H bend
65	1105.2	1044.9	1045	1042	A	ring deformation
66	1126.8	1083.6	1066	1066	A	C-H bend

67	1166.4	1091.7			A	C-H bend
68	1173.6	1100.7			A	C-H bend
69	1176.3	1109.7	1110		A	ring deformation
70	1206.9	1161.9	1142	1143	A	ring breathing
71	1223.1	1183.5			A	methyl CH wag
72	1236.6	1191.6	1164	1161	A	ring deformation
73	1244.7	1216.8			A	ring deformation
74	1248.3	1220.4	1175	1178	A	ring deformation
75	1255.5	1238.4		1193	A	methyl CH rock
76	1278.9	1251	1218	1220	A	molecular deformation
77	1310.4	1259.1	1252	1249	A	molecular deformation
78	1315.8	1264.5	1273		A	ring deformation
79	1331.1	1292.4	1292		A	ring deformation
80	1349.1	1328.4		1303	A	methyl CH rock
81	1363.5	1373.4			A	ring deformation
82	1404.9	1386.9	1325		A	ring deformation
83	1428.3	1406.7	1341	1342	A	molecular deformation
84	1438.2	1413.9			A	molecular deformation
85	1476	1439.1	1363	1359	A	ring stretch
86	1487.7	1459.8	1374		A	ring stretch
87	1497.6	1473.3	1385	1382	A	ring stretch
88	1514.7	1498.5			A	ring stretch
89	1551.6	1548.9	1411	1409	A	ring stretch
90	1580.4	1602.9		1440	A	molecular deformation + ring stretch
91	1592.1	1611.9		1567	A	ring stretch
92	1602	1613.7	1575		A	ring stretch
93	1604.7	1619.1	1595		A	ring stretch
94	1611.9	1625.4	1602	1600	A	ring stretch
95	1623.6	1640.7	1616	1616	A	C=C stretch
96	1824.3	1763.1	1665		A	C=O stretch antisym
97	1829.7	1770.3		1652	A	C=O stretch symm
98	2731.5	2694.6			A	methyl CH stretch
99	2748.6	2712.6			A	methyl CH stretch
100	2832.3	2718	2921	2919	A	methyl CH stretch
101	2846.7	2743.2	2966		A	C-H stretch
102	2853.9	2745			A	C-H stretch

103	2855.7	2746.8	3013	3015	A	C-H stretch
104	2856.6	2748.6		3037	A	C-H stretch
105	2862	2754.09	3044		A	C-H stretch
106	2864.7	2754.36			A	C-H stretch
107	2865.6	2755.8	3065		A	C-H stretch
108	2867.4	2762.1			A	C-H stretch
109	2870.1	2766.6	3074		A	C-H stretch
110	2874.6	2767.5		3078	A	C-H stretch
111	2878.2	2848.5	3082		A	C-H stretch

## APPENDIX B

### Synthesis of 8,13-benzo[a]naphthacenedione and 7-methyl-8,13-benzo[a]naphthacenedione

Experimental details follow the ones reported for Q1, Q2, and Q3 [1].

Figure 2.1 is a proposed schematic of the synthesis.

**1,3-Dihydro-1-hydroxy-3-methylnaphtho[1,2-c]furan, 3.** *n*-Butyllithium (20.1 mL of a 2.5 M solution in hexanes, 50 mmol) was added dropwise under nitrogen to 6.0 g (25 mmol) of **1** in 200 mL dry diethyl ether at -70°C. The mixture was stirred vigorously for 15 minutes, then warmed to 0°C. Dry DMF (2.5 mL, 32 mmol) was added dropwise, and the mixture was stirred for 16 h, gradually warming to room temperature. The reaction was quenched with water, the organic layer separated, washed twice with NH<sub>4</sub>Cl, dried with MgSO<sub>4</sub>, filtered, and the solvent was removed under reduced pressure. The crude product was dissolved in toluene, and crystallized by slow diffusion with hexane vapours (90 h) to give 2.0 g of a white solid. The NMR showed a diastereomeric mixture of **3** (39%): m.p. 107.5-108.5°; <sup>1</sup>H NMR (250 MHz, CDCl<sub>3</sub>) δ 1.54 (d, 6H, trans CH<sub>3</sub>), 1.65 (d, 6.5H, cis CH<sub>3</sub>), 3.13 (br s, 1H), 5.39 (q, 6.5H, cis CHCH<sub>3</sub>), 5.67 (dq, d=2.6, q=6, trans CHCH<sub>3</sub>), 6.84 (br s, cis CHOH), 6.93 (br s, trans CHOH), 7.31 (d, J=8 Hz, 1H), 7.4-7.6 (m, 2H), 7.8-7.9 (m, 2H), 8.0-8.1 (m, 1H); <sup>13</sup>C NMR (62.5 MHz, CDCl<sub>3</sub>) δ 21.60, 23.79, 79.49, 80.21, 100.52, 101.08, 118.68, 118.81, 123.82, 123.90, 125.85, 125.89, 127.10, 127.13, 128.42, 128.45, 130.41, 133.34, 133.37; IR (Nujol) 3410 (Br OH), 1439, 1069, 1017, 845 cm<sup>-1</sup>.

Analysis calculated for C<sub>13</sub>H<sub>12</sub>O<sub>2</sub>: C, 77.98; H, 6.04; found: C, 77.88; H, 6.17.

**7,14-Epoxy-7,7a,13a,14-tetrahydro-7-methyl-8,13-naphthacenedione.** 0.30 g (1.5mmol) of **3**, 0.355g (2.2 mmol) of 1,4-naphthoquinone, and a catalytic amount of *p*-toluenesulfonic acid monohydrate were refluxed in 50 mL of diethyl ether for 20 minutes, and then immediately cooled in a freezer. The crude product

(white precipitate) was filtered off, washed, and recrystallized from a mixture of ethyl acetate and petroleum ether, giving **5**. m.p. 165-6° <sup>1</sup>H NMR (250 MHz, CDCl<sub>3</sub>) δ 2.19 (s, 3H), 3.49 (d, J=8.7 Hz, 1H), 4.04-4.10 (m, 1H), 6.28 (d, J=5.4 Hz, 1H), 7.06-7.09 (m, 3H), 7.27-7.35 (m, 3H), 7.45-7.58 (m, 3H), 7.73 (d, J=8.3 Hz, 1H); <sup>13</sup>C NMR (62.5 MHz, CDCl<sub>3</sub>) δ 194.25, 193.75, 141.64, 139.30, 133.91, 133.77, 133.50, 133.18, 132.54, 128.40, 127.95, 127.05, 126.02, 125.61, 125.16, 123.73, 117.62, 91.63, 80.37, 55.44, 52.25, 17.11; IR (Nujol) 1674 (C=O), 1588, 1287, 1271, 978, 750 cm<sup>-1</sup>.

Analysis calculated for C<sub>23</sub>H<sub>16</sub>O<sub>3</sub>: C, 81.16; H, 4.74; found: C, 81.09; H, 4.92.

**7-Methyl-8,13-benzo[a]naphthacenedione**. To 50 mL dry diethyl ether at 0°C the following were added: 0.075g (0.22mmol) of **5**, and 0.050g (0.44mmol) of potassium-t-butoxide. The mixture was stirred for 24 h, and a brown precipitate was filtered. Recrystallization of the crude product from CHCl<sub>3</sub>/methanol gave 0.027 g of **7** (34%): m.p. 238°; <sup>1</sup>H NMR (250 MHz, CDCl<sub>3</sub>) δ 9.51 (s, 1H), 8.84 (d, J=1 Hz, 4.05H), 8.15-8.31 (m, 3H), 7.62-7.91 (m, 6H), 3.20 (s, 3H); <sup>13</sup>C NMR (62.5 MHz, CDCl<sub>3</sub>) δ 185.59, 183.49, 141.00, 136.13, 135.16, 134.07, 133.31, 132.40, 130.93, 130.72, 130.42, 128.52, 128.34, 127.76, 127.40, 126.66, 124.09, 123.01, 122.15, 17.12; IR (Nujol) 1665(C=O), 1362, 1291, 1273, 712 cm<sup>-1</sup>.

Analysis calculated for C<sub>23</sub>H<sub>14</sub>O<sub>2</sub>: C, 85.69; H, 4.38; found: C, 85.47; H, 4.45.

**7,14-Epoxy-7,14-dihydro-8,13-benzo[a]naphthacenedione, 4**. Hemiacetal **2**<sup>1</sup> (0.50 g, 2.7 mmol) and 1,4-naphthoquinone (0.425 g, 2.7 mmol) were refluxed in 25 mL of diethyl ether with a crystal of p-toluenesulfonic acid. After 2 hours, an additional 115 mg of 1,4-naphthoquinone was added and refluxing continued for another 2 hours. The reaction was cooled and filtered off resulting in 0.614 g of a white precipitate, endo **4**. The filtrate was washed with sodium bicarbonate solution, dried over MgSO<sub>4</sub> and filtered. The volume was reduced on a steam bath and petroleum ether was added. Cooling gave 0.124 g of a 2:1 endo:exo mixture



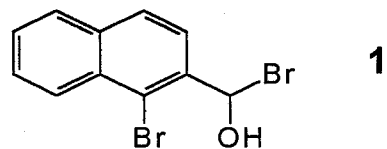
of adducts making the total yield 0.74 g (84%): the endo product had m.p. 161° (dec); <sup>1</sup>H NMR (250 MHz, CDCl<sub>3</sub>) δ 3.90-3.95 (m, 2H), 5.99 (d, J=4.4 Hz, 1H), 6.35 (d, J=4.3 Hz, 1H), 7.08-7.19 (m, 3H), 7.25-7.32 (m, 3H), 7.42-7.50 (m, 2H), 7.58 (d, J=7.7 Hz, 1H), 7.72 (d, J=8.3 Hz, 1H); <sup>13</sup>C NMR (62.50 MHz, CDCl<sub>3</sub>) δ 49.77, 50.78, 81.83, 83.76, 18.76, 123.82, 125.47, 125.69, 126.12, 126.50, 127.04, 128.02, 128.32, 132.55, 133.47, 133.62, 133.87, 139.00, 139.98, 193.45, 194.40; IR (Nujol) 1674 (C=O), 1586, 1269, 943, 799, 743 cm<sup>-1</sup>; MS (EI) *m/e* 326 (M<sup>+</sup>, 90), 308 (10), 297 (20), 252 (25), 239 (55), 181 (60), 168 (90), 158 (85), 139 (100).

Analysis calculated for C<sub>22</sub>H<sub>14</sub>O<sub>2</sub>: C, 80.97; H, 4.32; found: C, 80.87; H, 4.43.

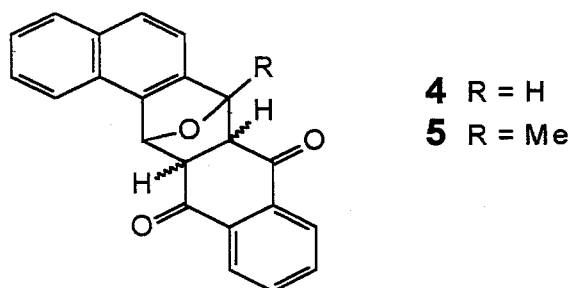
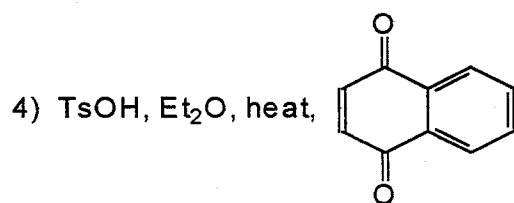
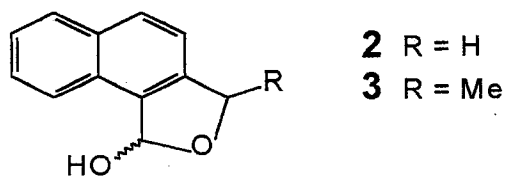
**8,13-Benzo[a]naphthacenedione, 6.** This compound was prepared from **4** in the same manner as **5**: m.p. 288°; <sup>1</sup>H NMR (250 MHz, CDCl<sub>3</sub>) δ 7.70-7.98 (m, 7H), 8.39-8.45 (m, 2H), 8.84 (s, 1H), 8.93 (d, J=8.44 Hz, 1H), 9.65 (s, 1H); <sup>13</sup>C NMR (62.5 MHz, CDCl<sub>3</sub>) δ 123.45, 123.92, 127.19, 127.40, 127.49, 127.90, 128.56, 128.96, 129.02, 130.26, 130.49, 130.83, 133.07, 133.57, 133.60, 134.15, 134.17, 134.26, 134.36, 135.05, 183.07, 183.17; IR (Nujol) 1669 (C=O), 1586, 1289, 822, 716, 706 cm<sup>-1</sup>; MS (EI) *m/e* 309 (M<sup>+</sup>+1, 24), 308 (M<sup>+</sup>, 100), 280 (14), 252 (21), 250 (17), 140 (9), 126 (18), 125 (16).

Analysis calculated for C<sub>22</sub>H<sub>12</sub>O<sub>2</sub>: C, 85.70; H, 3.92; found: C, 85.52; H, 3.97.

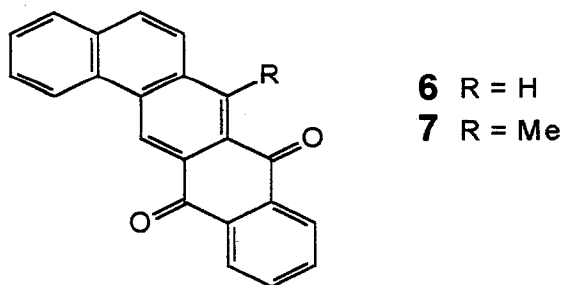
Figure 2.1  
Proposed schematic for synthesis of Q5, Q6



- 1) 2.1 equivalents n-BuLi, Et<sub>2</sub>O, -78°C → 0°C
- 2) DMF
- 3) H<sub>2</sub>O



- 5) K<sup>+</sup> O<sup>-</sup>-t-Bu, Et<sub>2</sub>O



Reference - Appendix B

- 1 James G. Smith, Peter W. Dibble and Richard E. Sandborn, *J. Org. Chem.* **1986**, *51*, 3762.

## **Vita Auctoris**

### **William J. Price**

William Price was born in Windsor, Ontario on August 11, 1969. He graduated from General Amherst High School in 1987 with top honours. After attending York University for a few years he returned to Windsor and received his Honours Bachelor of Science in Chemistry. He proceeded to enter the graduate program at the University of Windsor and is expected to receive his diploma for Master of Science in Chemistry in the fall of 1998. He has since proceeded to enter the graduate program at Wayne State University in Detroit, Michigan for a Doctor of Philosophy degree.